Edited by
Jonathan Gillard
Adam Waldman and
Peter Barker

Clinical MR Neuroimaging

Diffusion, Perfusion and Spectroscopy

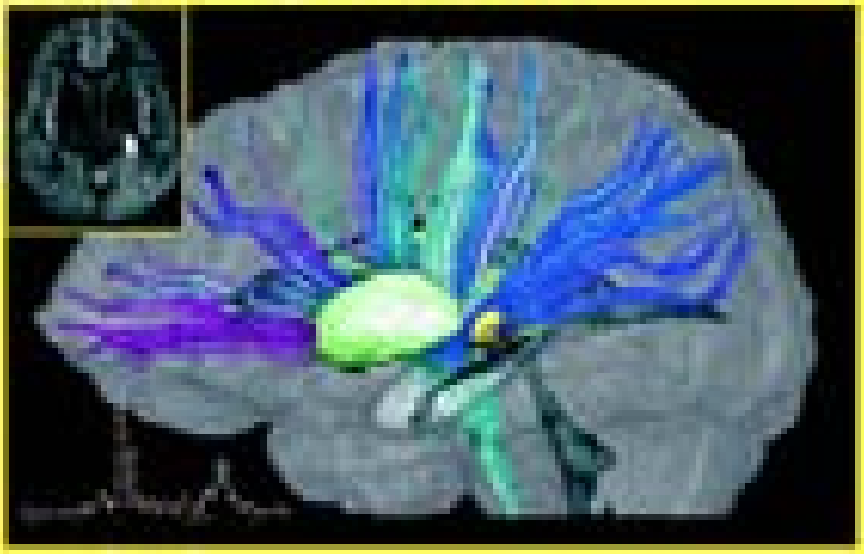

CAMBRIDGE

CAMBRIDGE www.cambridge.org/9780521824576

This page intentionally left blank

Clinical MR Neuroimaging

Diffusion, Perfusion and Spectroscopy

The physiological magnetic resonance (MR) techniques of diffusion imaging, perfusion imaging and spectroscopy offer insights into brain structure, function and metabolism. Until recently, these were mainly applied within the realm of medical research but, with their increasing availability on clinical MR imaging (MRI) machines, they are now entering clinical practice for the evaluation of neuropathology. This book provides the reader with a thorough review of the underlying physical principles of each of these methods, as well as comprehensive coverage of their clinical applications. Topics covered include single- and multiple-voxel MRS techniques; MR perfusion based on both arterial spin labeling and dynamic bolus tracking approaches; and diffusion-weighted imaging, including techniques for mapping brain white-matter fiber bundles. Clinical applications are reviewed in depth for each technique, with case reports included throughout the book. Attention is also drawn to possible artifacts and pitfalls.

To Susan for making it happen,
and Charlotte and Emily for making it worthwhile

JHG

To Jess, Ella and Danny

ADW

To Naomi, Catherine and Stephanie for their
patience and support during the preparation of this book

PBB

Clinical MR Neuroimaging

Diffusion, Perfusion and Spectroscopy

Edited by

Jonathan H. Gillard

Department of Radiology, University of Cambridge, UK

Adam D. Waldman

Department of Imaging, Charing Cross Hospital, London, UK
Institute of Neurology and Imperial College of Science, Technology and Medicine, London, UK

Peter B. Barker

Department of Radiology, Johns Hopkins University School of Medicine, Baltimore, USA

CAMBRIDGE UNIVERSITY PRESS

CAMBRIDGE UNIVERSITY PRESS
Cambridge, New York, Melbourne, Madrid, Cape Town, Singapore, São Paulo

Cambridge University Press
The Edinburgh Building, Cambridge CB2 8RU, UK

Published in the United States of America by Cambridge University Press, New York

www.cambridge.org
Information on this title: www.cambridge.org/9780521824576

First published in print format 2004

ISBN-13 978-0-511-26447-4 eBook (EBL)
ISBN-10 0-511-26447-X eBook (EBL)

ISBN-13 978-0-521-82457-6 hardback
ISBN-10 0-521-82457-5 hardback

Contents

List of Case Studies

Contributors

Dr. Elfar Adelsteinsson,
SRI International,
Room BN 168,
333 Ravenswood,
Menlo Park, CA 94025,
USA

Dr. Jeffry Alger,
University of California Los Angeles,
Ahmanson-Lovelace Brain,
Mapping Center Room 163,
660 Charles E Young Dr South,
Los Angeles, CA 90095-7085,
USA

Dr. Konstantinos Arfanakis,
Department of Biomedical Engineering,
Illinois Institute of Technology,
Chicago, IL 60616-3793,
USA

Dr. Peter B. Barker,
Department of Radiology, MRI 143C,
John Hopkins Medical Institutions,
600 N Wolfe Steet,
Baltimore, MD 21287,
USA

Dr. A. James Barkovich,
Department of Radiology L371,
University of California San Francisco,
505 Parnassus Avenue,
PO Box 0628,
San Francisco, CA 94143-0628,
USA

Dr. Alberto Bizzi,
Department of Neuroradiology,
Istituto Nazionale Neurologico,
Carlo Besta,
via Celoria 11,
Milano 20133,
Italy

Dr. Simona Bonavita,
Institute of Neurological Sciences,
Second University of Naples,
Piazza Miraglia 2,
Naples 80131,
Italy

Dr. Peter Bradley,
Division of Anaesthesia,
University of Cambridge,
PO Box 93, Level 4, E Block,
Addenbrooke's Hospital,
Hills Road, Cambridge, CB2 2QQ,
UK

Dr. Regula Briellmann,
Brain Research Institute,
Austin and Repatriation Medical Centre,
Banksia Street,
Heidelberg West, Victoria 3084,
Australia

Dr. Knut Brockmann,
Georg-August-Universitat,
Kinderklinik and Poliklinik,
Gottingen 37075,
Germany

Dr. William Brooks,
Departments of Neurology and Molecular and Integrative Physiology,
University of Kansas Medical Center,
3901 Rainbow Boulevard,
Kansas City, KS 66160,
USA

Dr. R. Nick Bryan,
Department of Radiology,
University of Pennsylvania Health System,
3400 Spruce Street,
Philadelphia, PA 19104,
USA

Dr. Marianna Bugiani,
Department of Neuroradiology,
Istituto Nazionale Neurologico,
Carlo Besta,
via Celoria 11,
Milano 20133,
Italy

Dr. Fernando Calamante,
Radiology and Physics Unit,
Institute of Child Health,
University College London,
30 Guilford Street,
London, WC1N 1EH,
UK

Dr. Linda Chang,
Department of Medicine,
University of Hawaii,
John A. Burns School of Medicine,
Honolulu, HI 96813,
USA

Dr. Thomas Chenevert,
Departments of Radiology and Biological Chemistry,
MSRB III, Room 9301,
1150 W Medical Center Dr,
Ann Arbor, MI 48109-0648,
USA

Dr. W. Kling Chong,
Department of Radiology,
Great Ormond Street Hospital,
Great Ormond Street,
London, WC1M 3JH,
UK

Serena Counsell,
Robert Steiner MR Unit,
Imaging Sciences Department,
Clinical Sciences Centre,
Imperial College,
Hammersmith Hospital,
London W12 OHS,
UK

Dr. Ugo Danesi,
Department of Neuroradiology,
Istituto Nazionale Neurologico,
Carlo Besta,
via Celoria 11,
Milano 20133,
Italy

Dr. Charles Davie,
Floor 3,
Royal Free and University College Medical School,
Rowland Hill Street,
London, NW3 2PF,
UK

Dr. Peter Dechent,
Biomedizinische NMR,
Forschungs GmbH am Max-Planck-Institut fur biophysikalische Chemie,
Gottingen 37070,
Germany

Dr. John Detre,
Departments of Neurology and Radiology,
University of Pennsylvania,
Philadelphia, PA 19104,
USA

Dr. Cathleen Enriquez,
Magnetic Resonance Spectroscopy,
Huntington Medical Research Institute,
660 South Fairoaks Avenue,
Pasadena, CA 91105,
USA

Dr. Thomas Ernst,
Department of Medicine,
University of Hawaii,
John A. Burns School of Medicine,
Honolulu, HI 96813,
USA

Dr. Christopher Fillipi,
Fletcher Allen Health Care-University of Vermont,
Department of Radiology,
Division of Neuroradiology,
111 Colchester Avenue,
Burlington, Vermont 05401

Dr. Massimo Filippi,
Neuroimaging Research Unit,
Scientific Institute and University,
Ospedale San Raffaele,
Via Olgettina 60,
Milan 20132,
Italy

Dr. Vijeya Ganesan,
Great Ormond Street Hospital for Children,
Great Ormond Street,
London, WC1N 3JH,
UK

Dr. Monika Garg,
Type V-B/3,
SGPGIMS Campus,
Raebareli Road,
Lucknow 226014,
India

Dr. Jonathan Gillard,
University Department of Radiology,
Addenbrooke's Hospital,
Cambridge, CB2 2QQ,
UK

Dr. Xavier Golay,
National Neuroscience Institute,
11 Jalan Tan Tock Jeng,
Singapore, 308433

Dr. R. Gilberto Gonzalez,
Department of Radiology,
Massachusetts General,
Hospital, Gray 2, Room B285,
55 Fruit Street,
Boston, MA 02114,
USA

Dr. Jeroen van der Grond,
Department of Radiology,
University Medical Center Utrecht,
Heidelberglaan 100,
Postbus 85500,
3508 Ga Utrecht,
The Netherlands

Dr. Rakesh Gupta,
Sanjay Gandhi Postgraduate Institute of
Medical Sciences,
Raebareli Road,
Lucknow 226014,
India

Dr. Folker Hanefeld,
Georg-August-Universitat,
Kinderklinik and Poliklinik,
Gottingen 37075,
Germany

Dr. Thomas Henry,
Department of Neurology,
Emory University,
Woodruff Memorial Building,
Suite 6000 PO Drawer V,
1639 Pierce Dr, Atlanta, GA 30322,
USA

Dr. Bruce Hermann,
Department of Neurology,
University of Wisconsin,
Madison, WI 53792,
USA

Dr. Jill Hunter,
E. B. Singleton Department of Diagnostic Imaging,
Texas Children's Hospital,
MC2-2521 6621 Fannin Street,
Houston, TX 77030,
USA

Dr. Ralph Hurd,
GE Medical Systems,
333 Ravenswood Avenue,
Building 307,
Menlo Park, CA 94025,
USA

Professor Clifford Jack,
Department of Radiology,
Mayo Clinic,
200 First Street SW,
Rochester, MN 55905,
USA

Professor Alan Jackson,
Imaging Sciences and Biomedical Engineering,
The Medical School,
University of Manchester,
Oxford Road, Manchester M13 9PT,
UK

Professor Graeme Jackson,
Brain Research Institute,
Austing and Repatriation Medical Centre,
Banksia Street,
Heidelberg West, Victoria 3084,
Australia

Dr. Derek Jones,
Section on Tissue Biophysics and Biomimetics,
Laboratory of Integrative Medicine and Biophysics,
National Institute of Child Health and Development,
Bethesda,
USA

Dr. Kejal Kantarci,
Department of Radiology,
Mayo Clinic,
200 First St SW,
Rochester, MN 55905,
USA

Dr. Shella Keilholz,
Laboratory of Functional and Molecular Imaging,
NINDS, NIH,
10/B1D118 MSC,
Bethesda, MD 20817,
USA

Dr. Martin Koch,
Universitatsklinikum Hamburg-Eppendorf,
Klinik und Poliklinik für Neurologie Martinistr 52,
20246 Hamburg,
Germany

Dr. Alan Koretsky,
Laboratory of Functional and Molecular Imaging,
NINDS, NIH,
10/B1D118 MSC,
Bethesda, MD 20817,
USA

Dr. Alexander Lin,
Magnetic Resonance Spectroscopy,
Huntington Medical Research Institute,
660 South Fairoaks Avenue,
Pasadena, CA 91105,
USA

Dr. Pratik Mukherjee,
Department of Radiology L371,
University of California San Francisco,
505 Parnassus Avenue,
PO Box 0628,
San Francisco, CA 94143-0628,
USA

Dr. Elias Melhem,
Department of Radiology,
University of Pennsylvania,
Health System,
3400 Spruce Street,
Pennsylvania, PA 19104,
USA

Professor David Menon,
Division of Anaesthesia,
University of Cambridge,
Box 93, Level 4, E Block,
Addenbrooke's Hospital,
Hills Road, Cambridge, CB2 2QQ
UK

Dr. Tom Mikkelsen,
Hermelin Brain Tumor Center,
Henry Ford Hospital, K-11,
Room W1138,
Grand Boulevard,
Detroit, MI 48202,
USA

Dr. Brad Moffat,
Departments of Radiology and Biological Chemistry,
MSRB III, Room 9301,
1150 W Medical Center Dr,
Ann Arbor, MI 48109-0648,
USA

Dr. Susumu Mori,
Department of Radiology,
Johns Hopkins Medical Institutions,
217 Traylor Building,
720 Rutland Avenue,
Baltimore, MD 21205-2195,
USA

Dr. David Norris,
FC Donders Centre for Cognitive Neuroimaging,
Trigon 181,
PO Box 9101,
6500 HB Nijmegen,
The Netherlands

Dr. Leif Østergaard,
Department of Neuroradiology,
CFIN, Arhus University Hospital,
Building 30,
Norrebrogade 44,
DK-8000 Aarhus C,
Denmark

Dr. Adolf Pfefferbaum,
SRI International,
Room BN 168,
333 Ravenswood,
Menlo Park, CA 94025,
USA

Professor John Pickard,
Academic Department of Neurosurgery,
Addenbrooke's Hospital,
PO Box 167,
Cambridge, CB2 2QQ,
UK

Dr. John Port,
Department of Radiology,
Mayo Clinic,
200 First Street SW,
Rochester, MN 55905,
USA

Dr. Luca Roccatagliata,
Department of Radiology,
Massachusetts General,
Hospital, Gray 2, Room B285,
55 Fruit Street,
Boston, MA 02114,
USA

Dr. Brian Ross,
Departments of Radiology and Biological Chemistry,
MSRB III, Room 9301,
1150 W Medical Center Dr,
Ann Arbor, MI 48109-0648,
USA

Dr. Brian Ross,
Magnetic Resonance Spectroscopy,
Huntington Medical Research Institute,
660 South Fairoaks Avenue,
Pasadena, CA 91105,
USA

Dr. Marco Rovaris,
Neuroimaging Research Unit,
Scientific Institute and University,
Ospedale San Raffaele,
Via Olgettina 60,
Milan 20132,
Italy

Dr. Dirk Rutgers,
Department of Radiology,
University Medical Center Utrecht,
Heidelberglaan 100,
Postbus 85500,
3508 Ga Utrecht,
The Netherlands

Dr. Mary Rutherford,
Robert Steiner MR Unit,
Imaging Sciences Department,
Clinical Sciences Centre,
Imperial College,
Hammersmith Hospital,
London W12 OHS,
UK

Dr. Dawn Saunders,
Great Ormond Street Hospital for Children,
Great Ormond Street,
London, WC1N 3JH,
UK

Dr. Pamela Schaefer,
Department of Radiology,
Massachusetts General,
Hospital, Gray 2, Room B285,
55 Fruit Street,
Boston, MA 02114,
USA

Dr. Afonso Silva,
Laboratory of Functional and Molecular Imaging,
NINDS, NIH,
10/B1D118 MSC,
Bethesda, MD 20817,
USA

Dr. Edith Sullivan,
SRI International,
Room BN 168,
333 Ravenswood,
Menlo Park, CA 94025,
USA

Dr. Lalith Talagala,
Laboratory of Functional and Molecular Imaging,
NINDS, NIH,
10/B1D118 MSC,
Bethesda, MD 20817,
USA

Professor Gioacchino Tedeschi,
Institute of Neurological Sciences,
Second University of Naples,
Piazza Miraglia 2,
Naples 80131,
Italy

Dr. Brian Tress,
Department of Radiology,
c/o PD Royal Melbourne Hospital,
Parkville, Victoria 3060,
Australia

Dr. Daniel Vigneron,
Department of Radiology L371,
University of California San Francisco,
505 Parnassus Avenue,
PO Box 0628,
San Francisco, CA 94143-0628,
USA

Dr. Adam D. Waldman,
Department of Imaging,
Charing Cross Hospital,
Fulham Palace Road,
London, W6 8RF,
UK

Dr. Jiongjiong Wang,
Departments of Neurology and Radiology,
University of Pennsylvania,
Philadelphia, PA 19104,
USA

Dr. Joanna Wardlaw,
Department of Clinical Neurosciences,
Western General Hospital,
Crewe Road,
Edinburgh,
Scotland

Professor K.M.A. Welch,
University of Kansas Medical,
Center, 8002 Wescoe,
3901 Rainbow Boulevard,
Mail Stop 1039,
Kansas City, KS 66160-7300,
USA

Dr. Mark Wellard,
Brain Research Institute,
Austin and Repatriation Medical Centre,
Banksia Street,
Heidelberg West, VIC. 3084,
Australia

Dr. Iain Wilkinson,
Academic Radiology C Floor,
Royal Hillamshire Hospital,
Glossop Road,
Sheffield, S10 2JF
UK

Dr. Peter van Ziji,
Department of Radiology,
Johns Hopkins Medical Institutions,
217 Traylor Building,
720 Rutland Avenue,
Baltimore, MD 21205-2095,
USA

Professor Robert Zimmerman,
Deparment of Radiology,
New York Hospital/Cornell,
525 E 68th Street,
New York, NY 10021,
USA

List of abbreviations

AA	Anaplastic astrocytoma
ABC	ATP-binding assette
ACA	Anterior cerebral artery
Ace	Acetate
AComA	Anterior communicating artery
AD	Alzheimer's disease
ADC	Apparent diffusion coefficient
ADEM	Acute disseminated encephalomyelitis
ADNFLE	Autosomal-dominant nocturnal frontal lobe epilepsy
ADP	Adenosine diphosphate
AED	Antiepileptic drugs
AFB	Acid fast bacilli
AFP	Adiabatic fast passage
AGAT	L-arginine : glycine amidinotransferase
a-glu	α-glucose
AIDS	Acquired immunodeficiency syndrome
AIF	Arterial input function
Ala	Alanine
ALD	Adrenoleukodystrophy
ALS	Amyotrophic lateral sclerosis
ANE	Acute necrotizing encephalopathy
ASA	Arylsulfatase A
ASL	Arterial spin labeling
ASPA	Aspartoacylase
ATLS	Advanced trauma and life support

ATP	Adenosine triphosphate
ATRT	Atypical terato-rhabdoid tumour
AUP	Area under peak
AVM	Arteriovenous malformations
AZT	Azidothymidine
BASING	Band-selective inversion with gradient dephasing
BAT	Bolus arrival times
BBB	Blood–brain barrier
BCAA	Branched-chain amino acids
BCKA	Branched-chain alpha-ketoacid
bFGF	Basic fibroblast growth factor
b-glu	β-glucose
BGT	Basal ganglia and thalami
BOLD	Blood oxygen level dependent
BVR	Basal vein of Rosenthal
CACH	Childhood ataxia with central hypomyelination
CADASIL	Cerebral autosomal dominant arteriopathy with subcortical infarcts and leukoencephalopathy
CASL	Continuous arterial spin labeling
CBD	Corticobasal degeneration
CBF	Cerebral blood flow
CBV	Cerebral blood volume
CE	Carotid endarterectomy
CEA	Carotid endarterectomy
CHESS	Chemical shift selective water suppression
Cho	Choline
CJD	Creutzfeldt–Jakob disease
CM	Chronic migraine
$CMRO_2$	Cerebral metabolic rate of oxygen metabolism
CNS	Central nervous system
CO	Carbon monoxide
COSY	Correlation spectroscopy
CPP	Cerebral perfusion pressure
Cr	Creatine
CSD	Cortical spreading depression
CSF	Cerebrospinal fluid
CSI	Chemical shift imaging
CT	Computed tomography
CTA	Computed tomography angiography
CTX	Cerebrotendinous xanthomatosis
CVR	Cerebrovascular reserve
DAI	Diffuse axonal injury
DANTE	Delays alternating with notations for tailored excitation
DAT	Dopamine uptake transporter
DEHSI	Diffuse excessive high signal intensity
DLB	Dementia with Long Bodies
DLPFC	Dorsolateral prefrontal cortex
DNA	Deoxyribonucleic acid
DNET	Dysembryoblastic neuroepithelial tumour
DRCE	Dynamic relaxivity contrast enhanced imaging
DRESS	Depth resolved surface coil spectroscopy
DRS	Disability rating scale
DRSTOT	Dementia rating scale total score
DSA	Digital subtraction angiography
DSCI	Dynamic susceptibility contrast imaging
DSM	Diagnostic and statistical manual of mental disorders
DTI	Diffusion tensor imaging
DWI	Diffusion-weighted imaging
DWIS	Diffusion-weighted imaging spectra
DZ	Dizygotic
EBV	Epstein–Barr virus
ECG	Electrocardiogram
EDAS	Encephaloduroarteriosynangiosis
EDE	Epidural empyemas
EDSS	Expanded disability status scale

EEG	Electroencephalograms
EES	Extravascular/extracellular space
EITB	Enzyme-linked immunotransfer blot
ELISA	Enzyme linked immunosorbent assay
EM	Episodic migraine
EPI	Echo planar imaging
EPISTAR	Echo planar imaging-signal tagging with alternating radio frequency
FA	Fractional anisotropy
FACT	Fiber assignment by continuous tracking
FADH	Flavin adenosine dinucleotide
FAIR	Flow-sensitive alternating inversion recovery
FAIRER	Flow-sensitive alternating inversion recovery with an extra radio frequency pulse
FASTMAP	Fast automatic shimming technique by mapping long projections
FDA	Food and drug administration
FDG	Fluoro-2-deoxyglucose
FEAST	Flow encoding arterial spin tagging
FEMN	"First episode, medication naive (schizophrenia)"
FGF	Fibroblast growth factor
FID	Free induction decay
FLAIR	Fluid attenuated inversion recovery
fMRI	Functional magnetic resonance imaging
FOV	Field of view
FSE	Fast spin echo
FT	Fourier transform
FTD	Frontotemporal degeneration
FWHM	Full width at half maximum
γ	Gyromagnetic ratios
GAA	Guanidinoacetate
GABA	γ-amino-butyric acid
GALC	Galactocerebroside β-galactosidase
GAMT	Guanidinoacetate methyl transferase
GBM	Glioblastoma multiforme
GCS	Glasgow coma scale
Gd-DTPA	Gadolinium dimeglumine gadopentetate
GE	Gradient echo
GFAP	Glial fibrillary acidic protein
GLD	Globoid cell leukodystrophy (Krabbe disease)
Gln	Glutamine
Glu	Glutamate
Glx	Glutamate and glutamine
Gly	Glycine
GM	Gray matter
GOS	Glasgow outcome score
GPC	Glycerophosphocholine
GPE	Glycerophosphoethanolamine
GRASS	Gradient recalled echo acquisition at steady state
GSS	Gerstmann–Straussler–Scheinker disease
HAART	Highly active antiretroviral therapy
HD	Huntington's disease
HIE	Hypoxic ischemic encephalopathy
HIV	Human immunodeficiency virus
HMPAO	Hexamethylpropyleneamine oxime
HPE	Holoprosencephaly
HS	Hippocampal sclerosis
HSCT	Hematopoietic stem cell transplantation
HSE	Herpes simplex encephalitis
HSV	Herpes simplex virus
ICA	Internal carotid artery
ICD	International classification of disease
ICP	Intracranial pressure
ILAE	International league against epilepsy
Ile	Isoleucine
ISIS	Image selective in vivo spectroscopy
IPD	Idiopathic Parkinson's disease
IVF	Interstitial volume fraction

IVIM	Intra voxel incoherent motion
JPA	Juvenile pilocytic astrocytoma
KD	Krabbe disease
KSS	Kearns–Sayre syndrome
Lac	Lactate
LACI	Lacunar infarction
LC model	Linear combination model
Leu	Leucine
LGN	Lateral geniculate nucleus
LHON	Leber's hereditary optic atrophy
LI	Lattice index
LR	Logistic regression
LS	Leigh syndrome
MB	Medulloblastomas
MCA	Middle cerebral artery
MCD	Myelinopathia centralis diffusa
MCI	Mild cognitive impairment
MCMD	Minor cognitive motor disorder
MEG	Magneto-encephalography
MEGA	Mescher–Garwood
MELAS	Mitochondrial encephalopathy with lactic acidosis and stroke
MERRF	Myoclonic epilepsy with ragged red fibers
mI	myo-inositol
MITR	Maximal intensity change per time interval ratio
MLC	Megalencephalic leukoencephalopathy with subcortical cysts
MLD	Metachromatic leukodystrophy
MMSE	Mini-mental state examination
MPC	Maximum peak concentration
MPCSI	Multi planar chemical shift imaging
MPRAGE	Magnetization prepared rapid acquisition gradient echo
MR	Magnetic resonance
MRA	Magnetic resonance angiography
MRI	Magnetic resonance imaging
MRS	Magnetic resonance spectroscopy
MRSI	Magnetic resonance spectroscopic imaging
MRUI	Magnetic resonance user interface
MS	Multiple sclerosis
MSA	Multisystem atrophy
MSM	Methylsulfonylmethane
MSUD	Maple syrup urine disease
MT	Magnetization transfer
MTC	Magnetization transfer contrast
MTI	Magnetization transfer imaging
MTR	Magnetization transfer ratio
MTT	Mean transit time
MZ	Monozygotic
NAA	*N*-acetyl aspartate
NAAG	*N*-acetyl aspartyl glutamate
NABT	Normal appearing brain tissue
NAGM	Normal appearing gray matter
NANA	*N*-acetylneuraminic acid
NASCET	North American symptomatic carotid endarterectomy trial
NAWM	Normal appearing white matter
NBV	Normalized brain volume
NF	Neurofibromatosis
NICE	National Institute of Clinical Excellence
NIHSS	National Institute of Health Stroke Scale
NINCDS–ADRDA	National Institute of Neurological and Communicative Disorders and Stroke–Alzheimer's Disease and Related Disorders Association
NKH	Non-ketotic hyperglycinaemia
NMR	Nuclear magnetic resonance
NOESY	Nuclear overhauser effect
NOS	Nitric oxide synthase
NTP	Nucleoside triphosphate

OCD	Obsessive compulsive disorder
OEF	Oxygen extraction fraction
OHG	Hydroxy glutaric acid
OphtA	Ophthalmic artery
OVS	Outer volume suppression
OXPHOS	Oxidative phosphorylation
PAC	Pulmonary artery catheter
PACE	Prospective acquisition and correction
PACI	Partial anterior circulation infarct
PAGM	Periaqueductal gray matter
PASL	Pulsed arterial spin labeling
PC	Phosphocholine
PCA	Posterior cerebral artery
PCD	Programmed cell death
PComA	Posterior communicating artery
PCR	Polymerase chain reaction
PCr	Phosphocreatine
PD	Proton density
PDE	Phosphodiester
PDGF	Platelet derived growth factor
PDS	Paroxysmal depolarization shifts
PET	Positron emission tomography
PGSE	Pulsed gradient spin echo
Phe	Phenylalanine
Pi	Inorganic phosphate
PKU	Phenylketonuria
PLIC	Posterior limb of the internal capsule
PLP	Proteolipid protein
PMD	Pelizaeus–Merzbacher disease
PME	Phosphomonoester
PML	Progressive multifocal leukoencephalopathy
PMN	Polymorphonuclear neutrophils
PNET	Primative neuroectodermal tumor
POCI	Posterior circulation infarct
POI	Pixel of interest
PP	Primary progressive (multiple sclerosis)
ppm	Parts per million
PRESS	Point resolved spectroscopy
PROBE	Proton brain exam
PROPELLER	Periodically rotated overlapping parallel lines with enhanced reconstruction
PS	Permeability surface
PSD	Periodic synchronous discharge
PSP	Progressive supranuclear palsy
PTA	Post traumatic amnesia
PTSD	Posttraumatic stress disorder
PVE	Partial volume effect
PVL	Periventricular leukomalacia
PWI	Perfusion weighted imaging
QUALY	Quality adjusted life years
QUIPSS	Quantitative imaging of perfusion using a single subtraction
QUIPSSII	Quantitative imaging of perfusion using a single subtraction II
RA	Relative anisotropy
RAA	Recently abstinent alcholics
rCBF	Relative cerebral blood flow
rCBV	Relative cerebral blood volume
RF	Radio frequency
RFA	Reduced flip angle
RN	Red nucleus
ROI	Region of interest
RPLS	Reversible posterior leukoencephalopathy syndrome
rR	Relative recirculation
RR	Relapsing–remitting (multiple sclerosis)
RT	Radiation therapy
rt-PA	Recombinant tissue plasminogen activator
SAT	Saturation

sCJD	Sporadic Creutzfeldt–Jakob disease
SD	Salla disease
SDE	Subdural empyema
SDH	Subdural hemorrhage
SDMT	Symbol digit modalities test
SE	Spin echo
SENSE	Sensitivity encoding
SI	Spectroscopic imaging
SIAM	Spectroscopic imaging acquisition mode
SLR	Shinnar–LeRoux
SLS	Sjogren–Larsson syndrome
SMIT	Na^+/myo-inositol cotransporter
SN	Substantia nigra
SNR	Signal-to-noise ratio
SOL	Space occupying lesion
SP	Secondary progressive (multiple sclerosis)
SPECT	Single photon emission computed tomography
SPM	Statistical parametric mapping
SRO	Steele–Richardson–Olszewski syndrome
SSPE	Subacute sclerosing panencephalitis
SSRIs	Selective serotonin reuptake inhibitors
STEAM	Stimulated echo acquisition mode
Suc	Succinate
SVD	Singular value decomposition
T_2W	T_2-weighted
TACI	Total anterior circulation infarct
TB	Tuberculosis
TBI	Traumatic brain injury
TCA	Tricarboxylic acid
TCD	Transcranial Doppler sonography
TDL	Tumefactive demyelinating lesions
TE	Echo time
TI	Inversion time
TIA	Transient ischemic attack
TLE	Temporal lobe epilepsy
TM	Transverse myelitis
TM	Mixing time
Tmax	Time to maximum peak
TMS	Transcranial magnetic stimulation
TOAST	Trial of Org 10172 in acute stroke treatment
TR	Repetition time
TS	Tuberous sclerosis
TSP	Trimethyl lysyl sodium propionate
TTFM	Time to first moment
TTP	Time to peak
UNFAIR	Perfusion imaging by un-inverted flow-sensitive alternating inversion recovery
USPIO	Ultra small particulates of iron oxide
VaD	Vascular dementias
Val	Valine
VC	Visual cortex
vCJD	Variant Creutzfeldt–Jakob disease
VEGF	Vascular endothelial growth factor
VHL	von Hippel–Lindau syndrome
VLCFA	Very long chain fatty acids
VOI	Volume of interest
VSS	Very selective saturation
VWM	Vanishing white matter disease
WET	Water suppression enhanced through T1 effects
WHO	World Health Organization
WI	Weighted images
WM	White matter
WMH	White matter hyperintensities
x-ALD	x linked adrenoleukodystrophy
Xe-CT	Xenon-enhanced computed tomography
ZDV	Zidovudine

Foreword

The advent of clinical MR imaging (MRI) in the 1980s heralded a new era in the ability to image the brain in vivo. MRI allows the detailed depiction of brain anatomy and pathology with unprecedented spatial resolution and soft-tissue contrast. It is also relatively safe and completely non-invasive. Nevertheless, the sensitivity and specificity with which structural MRI alone can define the wide range of neurological disease is limited.

The last decade has also seen the development of *physiological* MR techniques, whereby information concerning tissue *function* as well as structure is obtained. These techniques include diffusion, perfusion, and MR spectroscopy, which provide information on tissue ultra-structure, blood flow, and biochemistry, respectively. Information of this type supplements and complements that from clinical or structural imaging investigations, often providing important surrogate markers of disease pathophysiology or therapeutic response.

These techniques, previously only available in a research environment, are now accessible on most MR systems and can readily be incorporated into clinical imaging examinations. To date, however, there has been a paucity of literature in a single volume to support those wishing to apply physiological imaging studies in a clinical context. The aim of this book is to address the appropriate clinical application and interpretation of diffusion, perfusion, and spectroscopy.

The first section of the book describes the physical principles underlying each technique, as well as the potential associated artifacts and pitfalls.

The second section addresses applications in the different branches of clinical neuroscience. Chapters are grouped according to pathology, and are preceded by overviews that aim to place these methodologies in a broader clinical perspective. Illustrative case reports are included throughout the book.

We recognize that the term "functional MRI" (fMRI) has become synonymous with studies of localized brain activation, mostly using "blood oxygen level-dependent" (BOLD) contrast. This approach, which continues to contribute to the understanding of the relationship between brain structure and function, is well covered in other texts and is not addressed in this volume. Likewise, magnetization transfer imaging, and methods for post-processing structural data, for example volumetric analysis, or MRI relaxometry, are not included. While these techniques are the subject of much research effort, they are not widely available at the time of writing, and have yet to find a definitive clinical role.

The aim of this book is to create a reference work for those techniques that can be widely applied, not just at academic medical centers. Currently, diffusion, perfusion, and spectroscopy are the physiological techniques most likely to be used routinely. Our hope is that this book will provide a balanced reference work for physiological MRI in real clinical practice. The overall aim is to optimize the use of these techniques to increase the sensitivity and specificity of the MR imaging examination, and thereby improve the management of individual patients.

Jonathan H. Gillard, Cambridge
Adam D. Waldman, London
Peter B. Barker, Baltimore

Introduction

R. Nick Bryan

Department of Radiology, University of Pennsylvania Health System, 3400 Spruce Street, Philadelphia, USA

The last several decades have seen remarkable advances in the clinical neurosciences with some of the most remarkable achievements related to neuroimaging. Given the current depth of knowledge about the brain, it is difficult to appreciate that barely 300 years ago this organ was almost a complete mystery, particularly as to its function. While the brain has been recognized as an "organ" since antiquity, no functional role was ascribed to it until the early 1600s when Descartes placed the "soul" in one of its small parts, the pineal gland (Marshall and Magoun, 1998). Prior to this intriguing, but erroneous concept, much more functional importance had been attributed to the fluid in the ventricles than the brain itself. Descartes' non-scientific attribution was, fortunately, quickly followed by the much more rigorous description of the structure of the brain by Thomas Willis (1664). While Willis' application of the scientific method to the brain was seminal, the primitive scientific tools available at the time limited his direct observations to anatomy, which in and of itself does not convey function. Despite little direct evidence, Willis began to argue that mental functions reside in the brain, as do certain diseases such as epilepsy. The scientific tools necessary to prove his assertions by actual observation of physiology, molecular biology, and other "functional" aspects of the brain were still several centuries away.

However, the brain was found to have a peculiarly strong correlation between structure (anatomy) and function (behavior). This intimate relationship provided the basis for the still robust field of "experimental" neuroanatomy. Experimental neuroanatomy, such as the destruction of a portion of the brain in an animal followed by observations of its behavior allowed 18th and early 19th Century scientists such as Gall and Rolando to make structure/function correlations that documented the brain as a central control organ (Marshall and Magoun, 1998). Since it has never been appropriate to perform debilitating experiments on human beings, many fundamental questions pertaining to human brain function persisted until the "natural science" version of experimental neuroanatomy was introduced by clinicians such as Morgagni, who attributed neurological deficits such as hemiparesis to grossly destructive lesions of patients' brains found at autopsy (Morgagni, 1760). Broca, in 1860, applied such lesion/deficit correlation to a patient who had suffered the acute onset of aphasia and whose brain at autopsy revealed an infarct in the right frontal operculum, thus localizing a component of speech to a particular cortical region (Broca, 1861). Such "dysfunctional" imaging was subsequently employed by many clinical scientists, particularly those 19th and early 20th Century neurologists whose names are attached to so many neurological syndromes. While lesion/deficit correlation has been a very informative means of studying the brain, it is limited by its anatomic basis that does not provide any direct information about the brain's physiology or molecular makeup.

Note that all of these early methods of studying the brain involved some form of imaging. Given the spatially heterogeneous nature of the brain (both structurally and functionally), imaging of the brain is an absolute necessity in order to document the location of an experimental or natural lesion. Only with this anatomic information could the observed neurological, psychological, or cognitive dysfunction be linked to its physical source. In human

beings these types of investigations were severely restricted by the unfortunate necessity of a patient having to suffer an insult to the brain and the additional burden that the patient either die and have permitted an autopsy or submit to a craniotomy. These were until very recently the only means of directly documenting the presence and extent of a brain lesion.

Despite the many drawbacks, experimental anatomy and clinical lesion/deficit research in the first half of the 20th Century provided the basis of much of our current understanding of functional localization in the brain. During the second half of the 20th Century, these early, primitive, but informative techniques were increasingly supplemented by sophisticated histological, neurophysiological, and molecular biological techniques that have combined to yield the great depth of knowledge about the brain that we now have; knowledge that extends from single cell events to highly integrated cognitive functions. However, many of these newer techniques also have restrictions to their applications in human beings, particularly intact, functioning human beings. Histological techniques require tissue, never easily obtained from human brain and almost never from multiple or large regions. Many neurophysiological techniques require intrusion into the brain, as for electrode recordings or cortical stimulation. Molecular techniques are seldom feasible in intact functioning brain. While these powerful techniques provide extraordinarily detailed information about small parts of the brain, none provide data from the entire, functioning brain. This is a significant limitation as many functions of the brain involve composite actions of its many spatially, physiologically, and biochemically disparate components. This is particularly true of complex behavioral tasks and cognition. The spatial heterogeneity of the brain has always begged for imaging of the whole organ, preferably in the intact, functioning state. This has not been feasible until very recently.

In 1974 clinical neuroscience experienced a profound change with the invention of the X-ray computed tomography (CT) scanner, an instrument that for the first time could non-invasively produce images of the whole, living human brain (Hounsfield, 1973). CT scans are based on electron density and there are only subtle differences of this parameter in the brain. For instance, the electron density of gray matter (GM) and white matter (WM) differ by only 0.5%. Hence, clinical CT scans yield relatively crude images of the brain. While CT scanners can only image anatomy at a relatively low resolution it has allowed the traditional lesion/deficit methodology to be applied to living subjects contemporaneously with functional examinations. Autopsy and craniotomy are no longer necessary to demonstrate the anatomical correlates of functional deficits and the literature has become replete with lesion/deficit studies expanding our knowledge of how the function of the human brain is spatially distributed. Investigators such as the Damasio's have used clinical CT, and later magnetic resonance (MR) scans of hundreds of neurologically, psychologically, and cognitively impaired subjects to better demonstrate the anatomic substrate of higher order mental tasks (Damasio and Damasio, 1989). However these images still show only static anatomy and do not reflect any physiological or molecular aspect of the brain. Indeed it can be difficult to tell a conventional CT or MR scan of a cadaver's brain from that of a normal person. While we now understand many strong relationships between the gross structure and function of the brain, there remains the overpowering need to be able to directly "see" physiological and molecular function of the brain. After all, it is more important to know what the brain is doing than what it looks like!

This need was initially met by the combination of positron emission tomography (PET) and metabolic radio tracers such as $F^{18}DG$, H_2O^{15}, and CO^{15} (Fox *et al.*, 1988). PET methodology allows non-invasive imaging of the whole brain under resting as well as task conditions. Physiological parameters, such as cerebral blood flow (CBF) can be imaged non-invasively in the clinical environment, as can responses of these parameters to activation of the brain by a task – direct imaging of dynamic brain physiology. In addition, radio ligands have been developed that produce images of the distribution of specific molecules in the brain, such as components of neurotransmitter systems. This methodology remains a powerful research tool, albeit expensive and logistically challenging.

As a result of these advances, the 20th Century progressed from very limited, invasive anatomic

imaging of a poorly understood human brain to widely applied, non-invasive, dynamic physiological and biochemical imaging of a richly appreciated organ. Continuing advances in neuroimaging will offer ever more information about the brain and its function.

This book focuses on the important evolving methodology of MR imaging (MRI), specifically physiological MRI of the brain. MRI derived from nuclear MR (NMR), a physical phenomenon related to the behavior of nuclei in the presence of a magnetic field that was described by Felix Bloch, Hansen and Packard (1946). During the 1940s and 1950s many investigators developed techniques that allowed this physical phenomenon to be exploited for the study of chemical structure. Since the introduction of the Fourier transform (FT) technique by Ernst in 1966 and the development of high-field superconducting magnets, NMR has been able to elucidate the detailed chemical structure of even large molecules such as proteins (Ernst and Anderson, 1966). The addition of magnetic field gradients to the requisite static magnetic field of NMR can spatially define a sample, allowing MRI. This concept of the use of magnetic field gradients to generate images was first demonstrated in the landmark 1973 paper by Lauterbur; in 1976, Ernst introduced the principle of two-dimensional FT NMR which is now almost universally used for all MRI (Lauterbur, 1973; Aue *et al.*, 1976).

Conventional MRI relies on radio signals emitted by nuclei of molecules, particularly H_2O, of relatively stationary tissue. Because of their different water content and relaxation times, there is typically more than 20% difference in this signal between GM and WM. Similar differences can be found between certain pathological tissues and normal brain. This accounts for the exquisite images of normal neuroanatomy or multiple sclerosis (MS) plaques produced by contemporary MRI. The first decade of clinical MRI was characterized by steady improvements in the morphological imaging capabilities of this quite remarkable and completely non-invasive and safe technology. However, there is little useful physiological information in conventional MRI signal, except for that related to fast-flowing fluids such as blood. Recent MRI advances have focused on the development and application of molecular and physiological imaging capabilities. These new MRI methods are the subject of this volume and reflect the continuing evolution from purely anatomic to physiological and molecular imaging of the brain.

The three main physiological MR methods to be presented are MR spectroscopy (MRS), diffusion, and perfusion MRI. MRS yields images of the distribution and concentration of naturally occurring molecules such as *N*-acetyl aspartate (NAA) (one of the most abundant amino acids in the brain, and believed to be localized predominantly in neurons and their processes), choline (Cho) (a key constituent of cell membranes) and lactate (Lac) (a reflection of anaerobic metabolism). Diffusion MRI demonstrates regions of normal and pathological micromolecular motion. Under appropriate conditions, these images can reflect patterns of axonal anatomy and when applied as "fiber tracking" this technique can turn the large homogeneously bland regions of WM of conventional MRI into dramatic three-dimensional displays of the major axonal pathways. Using extrinsic contrast agents or intrinsic contrast agents, such as blood, perfusion MRI cannot only create qualitative, but quantitative maps of various perfusion parameters, including CBF, cerebral blood volume (CBV), and vascular permeability. With these techniques, at last, neuroscientists can painlessly, non-invasively, and safely study important physiological properties of a whole, living, functioning human brain. One can now actually see what the brain is doing, not just what it looks like.

The clinical value of these physiological and molecular tools is becoming increasingly appreciated and can be illustrated by their applications to one disease – cerebral ischemia and stroke. Lac is an important metabolic molecule of which little is produced by the brain under aerobic conditions. However, under anaerobic conditions, such as ischemia, abundant Lac may be produced and is easily detected by proton MRS (Barker *et al.*, 1994). The imaging of Lac by MRS is one of the most sensitive means of detecting even mild cerebral ischemia, its presence temporally preceding irreversible ischemia and stroke. Diffusion MRI is also very sensitive to ischemia, presumably because there is a shift of extracellular water molecules into the intracellular compartment where molecular diffusion is more

restricted (Le Bihan *et al.*, 1986). Even if this theory is not correct, empirically it is well established that diffusion weighted images show some of the earliest changes of stroke and severe ischemia. It almost goes without saying that perfusion imaging is a powerful tool for evaluating cerebral ischemia. Perfusion MRI can easily, directly, and accurately document the reduction of CBF secondary to obstructive or non-obstructive cerebral ischemia as well as demonstrate changes in CBV that often provide additional information as to the physiological severity of the insult (Rempp *et al.*, 1994). Such physiological tools are increasingly necessary for the management of acute cerebral ischemia when the traditional anatomic diagnosis of "live brain/dead brain" is not adequate for directing vascular or neuroprotective treatment.

The authors of the chapters of this book describe the latest physiological MRI methodologies in detail and then illustrate their applications to major diseases of the brain, including cerebrovascular and degenerative diseases, neoplasia, inflammation, trauma, and even psychiatric disorders. These new techniques of the early 21st Century foreshadow even more remarkable advances in neuroimaging, but first, please appreciate the robust functional imaging capabilities so well described and illustrated in this volume.

REFERENCES

Aue WP, Bartholdi E, Ernst RR. 1976. Two-dimensional spectroscopy. Application to nuclear magnetic resonance. *J Chem Phys* 64: 2229.

Barker PB, Gillard JH, van Zijl PCM, *et al*. 1994. Acute stroke: evaluation with serial proton magnetic resonance spectroscopy. *Radiology* 192: 723–732.

Bloch F, Hansen WW, Packard M. 1946. The nuclear induction experiment. *Phys Rev* 70: 474–485.

Broca P. 1861. Remarques sur le siège de la faculté du langage articule, suivies d'une observation d'aphémie. *Bull Soc Anat Paris*: 330–357. Trans. Von Boninn G. *Some Papers on the Cerebral Cortex*. Springfilld. Ill. C.C. Thomas, 1960.

Damasio H, Damasio AR. 1989. *Lesion Analysis in Neuropsychology*. Oxford University Press, NY, USA.

Ernst RR, Anderson WA. 1966. *Rev Sci Instrum* 37: 93.

Fox PF, Raichle ME, *et al*. 1988. Nonoxidative glucose consumption during focal physiologic neural activity. *Science* 241: 462–464.

Hounsfield GN. 1973. Computerized transverse axial scanning (tomography): part 1. description of system. *Br J Radiol* 46: 1016–1022.

Lauterbur PC. 1973. Image formation by induced local interactions: examples employing nuclear magnetic resonance. *Nature* 242: 190–191.

Le Bihan D, Breton E, Lallemand D. 1986. MR imaging of intravoxel incoherent motions: application to diffusion and perfusion in neurologic disorders. *Radiology* 161: 401–407.

Marshall LH, Magoun HW. 1998. *Discoveries in the Human Brain*. Humana Press Inc, Totowa, NJ, USA.

Morgagni JB. 1760. *The Seats and Causes of Diseases*. Trans. Alexander B. The Classics of Medicine Library, Birmingham, AL, USA.

Rempp KA, Brix G, Wenz F, Becker CR, Guckel F, Lorenz WJ. 1994. Quantification of regional cerebral blood flow and volume with dynamic susceptibility contrast-enhanced MR imaging. *Radiology* 193: 637–641.

Willis T. 1664. *Cerebri Anatome*. Trans. Pordage S. The Classics of Medicine Library, Birmingham, AL, USA.

Section 1

Physiological MR techniques

1

Fundamentals of MR spectroscopy

Peter B. Barker

Department of Radiology, Johns Hopkins University, School of Medicine, Baltimore, USA

Introduction

Nuclear MR (NMR) spectroscopy in bulk matter was demonstrated for the first time in 1945 when Bloch and Purcell independently demonstrated that a strong magnetic field induced splitting of the energy levels and detected the resonance phenomena (Bloch, 1946; Purcell *et al.*, 1946). The method was originally of interest only to physicists for the measurement of gyromagnetic ratios (γ) of different nuclei, a constant specific to a particular nucleus, but applications of NMR to chemistry became apparent after the discovery of chemical shift and spin-spin coupling effects in 1950 and 1951, respectively (Proctor and Yu, 1950; Gutowsky *et al.*, 1951). The spectra of high-resolution liquid NMR contain fine structure information because the nuclear resonance frequency is influenced by both neighboring nuclei and the chemical environment which allows information on the structure of the molecule to be deduced. Hence, NMR spectroscopy rapidly became an important, and widely used, technique for chemical analysis and structure elucidation of chemical and biological compounds.

Major technical advances in the 1960s included the introduction of superconducting magnets (1965), which were very stable and allowed higher field strengths than with conventional electromagnets to be attained, and in 1966 the use of the Fourier transform (FT) for signal processing. In nearly all contemporary spectrometers, the sample is subjected to periodic radio frequency (RF) pulses directed perpendicular to the external field and the signal is Fourier transformed to give a spectrum in the frequency domain. FT NMR provides increased sensitivity compared to previous techniques, and also led to the development of a huge variety of pulsed NMR methods, including multi-dimensional NMR techniques.

Biological and medical applications of MR were developed in the early 1970s with the introduction of MR imaging (MRI) and MR spectroscopy (MRS) of biological tissue. In vivo MRS of humans became possible in the early 1980s with the advent of whole body magnets with sufficiently high field strength and homogeneity (Radda, 1986). Early studies focused on the phosphorus nucleus, since this was the most technically feasible at that time. Methods were developed for spatially localized ^{31}P MRS (Luyten *et al.*, 1989), and studies of major neuropathology (such as stroke or brain tumors) were performed (Arnold *et al.*, 1989; Cadoux *et al.*, 1989; Levine *et al.*, 1992). A significant problem with ^{31}P MRS, however, is its low sensitivity (mainly because of the relatively low γ of ^{31}P, and low concentrations of phosphorus containing compounds). Since the spatial resolution in in vivo spectroscopy is largely limited by the signal-to-noise ratio (SNR) the minimum voxel size for ^{31}P spectroscopy of the human brain is typically 30 cm^3 using conventional techniques and 1.5 T magnets. The technique can therefore only be applied to either very large lesions, diffuse or global diseases.

In recent years, there has been more interest in proton MRS, particularly after it was demonstrated that it was possible to obtain high-resolution spectra from small, well-defined regions in reasonably short scan times (Frahm *et al.*, 1989). The higher sensitivity of the proton is due to several factors, including higher γ, higher metabolite concentrations, and

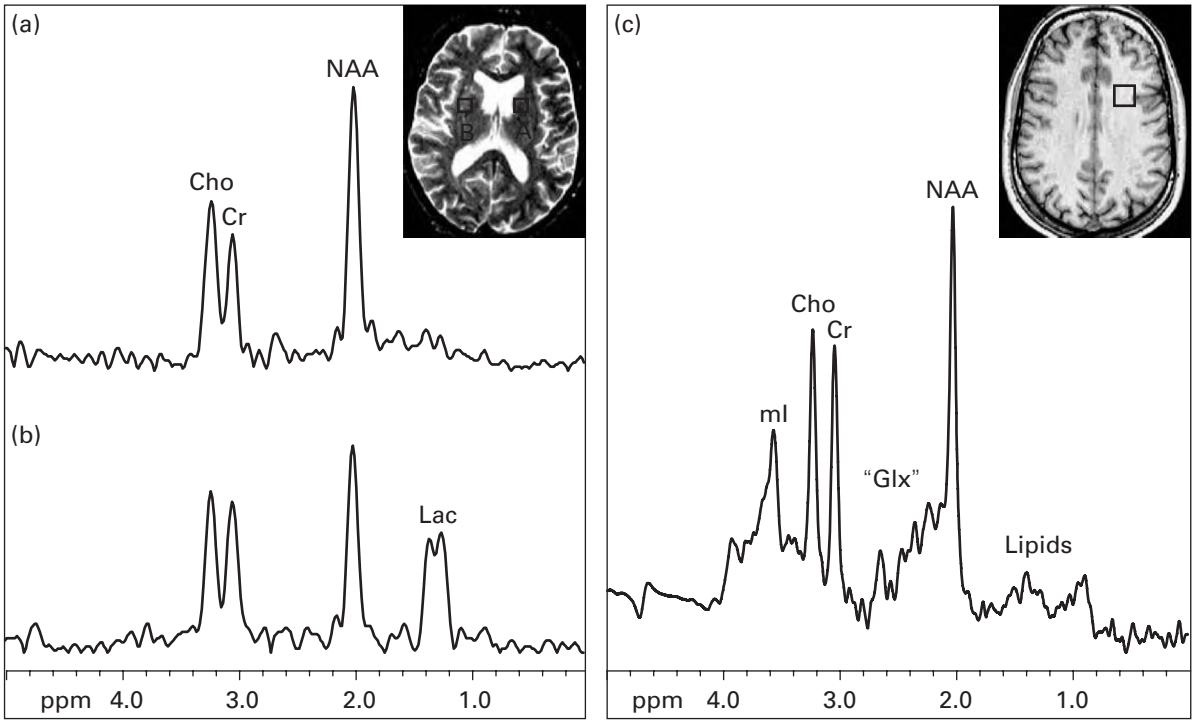

Fig. 1.1 Proton spectra of the human brain recorded at both (a, b) long (TE 272) and (c) short (TE 35 ms) TEs, in the long TE spectra from a patient with an acute right middle cerebral artery (MCA) stroke, the normal spectrum (a) from the left hemisphere shows signals from Choline (Cho), Creatine (Cr) and N-acetyl aspartate (NAA). In the ischemic left hemisphere (b) an additional signal due to Lactate (Lac) is apparent as well as a moderate decrease in NAA. In the short TE spectrum of normal frontal WM (c), in addition to NAA, Cr and Cho, signals can be detected from myo-inositol (mI), Glutamate and Glutamine (Glx), and lipids. (a) and (b) are from a multi-slice MR spectroscopic imaging (MRSI) data set (nominal voxel size 0.8 cm^3), while (c) is recorded from an 8 cm^3 single voxel using the Point resolved spectroscopy (PRESS) sequence.

more favorable relaxation times. Although proton spectroscopy has been demonstrated in a number of organ systems (in particular, recent studies show promise for the use of proton spectroscopy in the diagnosis of prostate and breast cancer), the overwhelming number of applications have been in the brain, because of the absence of free lipid signals in normal cerebrum, relative ease of shimming, and lack of motion artifacts. The proton is also a widely used nucleus because it is the same nucleus used for conventional MRI, and therefore it is usually possible to perform proton MRS on most 1.5 T or higher clinical MRI machines without the need to purchase additional scanner hardware or modifications.

NMR spectroscopy can in fact be performed with many different nuclei, and in the brain, in addition to ^{1}H and ^{31}P, there have been reports of spectroscopy of deuterium (^{2}D), carbon-13, nitrogen-15, lithium-7, sodium-23, and fluorine-19, using either signals from endogenous nuclei and/or compounds, or via the administration of (sometimes isotopically enriched) exogenous substances. All of these studies fall into the context of advanced research at the current time, and therefore will not be considered further here. This chapter focuses on the information content of proton MR spectra of the brain, technical issues such as choice of localization technique, and normal age-related and anatomical variations.

Information content of proton MR spectra of the brain

Figure 1.1 shows examples of proton spectra recorded at long and short echo times (TEs). The assignment and significance of each the resonances in the spectrum is discussed below, and summarized in Table 1.1.

Table 1.1. Metabolites detected in the brain by proton MR spectoscopy

Metabolite	Chemical shift normal concentration median (range)	Physiological significance	Increased	Decreased
NAA (NAA, other *N*-acetyl moieties)	2.02 ppm 7.8 mM (6.5–9.7)	Health neuronal cell marker. Only seen in nervous tissue. Exact physiological role uncertain.	v.rarely Canavan's disease	Commonly: non-specific neuronal loss or dysfunction due to range of insults. Incl. Ischaemia, trauma, inflammation, infection, tumors, dementia, gliosis.
Cho Cho-containing compounds	3.2 ppm 1.3 mM (0.8–1.6)	Detectable resonance is predominantly free Cho and derivatives. Marker of membrane turnover. Higher in W.M. than G.M. Increase with age.	Tumors, inflammation, chronic hypoxia,	Stroke, encephalopathy (hepatic human immunodeficiency virus (HIV)/liver disease.
Cr Creatine/ phosphocreatine	3.0 ppm 4.5 mM (3.4–5.5)	Compounds related to energy storage; thought to be marker of energetic status of cells. Other metabolities are frequently expressed as ratio to Cr. Low in infants. Increases with age.	Trauma, hypersomolar states	Hypoxia, stroke, tumors
Myo Myo-inositol (mI) (other inositols)	3.56 ppm (short TE only) 3.8 mM (2.2–6.8)	Pentose sugar. Involved in inositol triphosphate intra-cellular second messenger cycle, osmolyte, glial cell marker. High in infants.	Neonates, Alzheimer's disease, diabetes, recovered encephalopathy, low grade glioma, hyperosmolar	Malignant tumors, Chronic hepatic encephalopathy, stroke
Glx Glutamate (Glu)/ Glutamine(Gln)	2.1–2.4 ppm (short TE only) Glu ~ 10 mM Gln ~ 5 mM	Complex overlapping J-coupled resonances difficult to separate and quantify at clinical field strengths (1.5–3 T). Amino acid neurotransmitters Glu excitatory, Gln inhibitory.	Hepatic encephalopathy, severe hypoxia, OTC deficiency	Possibly Alzheimer's disease
Lactate	1.35 ppm (doublet, 7 ppm separation) Detectable >~1 mM	Not seen in normal brain. End product of anaerobic respiration. May be energetic substrate of much brain metabolism. Thought to be elevated in foamy macrophages.	Ischaemia, inborn errors of metabolism (especially respiratory chain defects, tumors (all grades)), abscesses, inflammation.	
Lipids Mobile liquid moieties	0.9 and 1.3 ppm (short TE unless(↑↑))	Not seen in normal brain. Membrane breakdown/lipid droplet formation. May precede histological necrosis.	High-grade tumors, abscesses, acute inflammation, acute stroke.	
Succinate, acetate, amino acids	Various Not normally detectable	Products of bacterial metabolism.	Pyogenic abcesses. Alanine: meningiomas	
Acetoacetate, acetone		Intermediary metabolites only pathologically elevated in inborn errors.	Inborn errors of metabolism	
Mannitol, ethanol	Various	Administered drugs and other substances		

N-acetyl aspartate

The largest metabolite signal, resonating at 2.02 ppm, occurs from the *N*-acetyl group of *N*-acetyl aspartate (NAA), with perhaps a small contribution from *N*-acetyl aspartyl-glutamate (NAAG) (Frahm *et al.*, 1991). Despite being one of the most abundant amino acids in the central nervous system (CNS), NAA was not discovered until 1956 and its function has been the subject of considerable debate. It has been speculated to be a source of acetyl groups for lipid synthesis, a regulator of protein synthesis, a storage form of acetyl-CoA or aspartate, a breakdown product of NAAG, a "molecular water pump", or an osmolyte (Barker, 2001). Using immunocytochemical techniques, NAA has been shown to be predominantly localized to neurons, axons, and dendrites within the central nervous system (Simmons *et al.*, 1991), and studies of diseases known to involve neuronal and/or axonal loss (e.g. infarcts, brain tumors, seizure foci, multiple sclerosis (MS) plaques) have uniformly shown NAA to be decreased. In pathologies, such as MS, correlations between brain levels and clinical measures of disability have been shown (De Stefano *et al.*, 2001). Animal models of chronic neuronal injury have also been shown to give good correlations between NAA levels (as measured by MRS) and in vitro measures of neuronal survival (Simmons *et al.*, 1991; Guimaraes *et al.*, 1995).

For all these reasons, it has been tempting to "label" NAA as a neuronal marker, and to equate levels of NAA with neuronal density. However, there is increasing evidence that this may not be the case. NAA has been detected in non-neuronal cell types, such as mast cells or isolated oligodendrocyte preparations, suggesting that NAA may not be specific for neuronal processes (Urenjak *et al.*, 1992; Burlina *et al.*, 1997, Bhakoo and Pearce, 2000), although it is not completely clear if these cells are present in the brain or high concentrations, or if their metabolism is identical, in vivo. It is also well known that there are exceptions to the correlation between neuronal density and NAA levels. For instance, the pediatric leukoencephalopathy (Canavan's disease) is associated with a large elevation of intracellular NAA, owing to deficiency of aspartoacylase (ASPA), the enzyme that degrades NAA to acetate and aspartate (Figure 1.2) (Barker *et al.*, 1992).

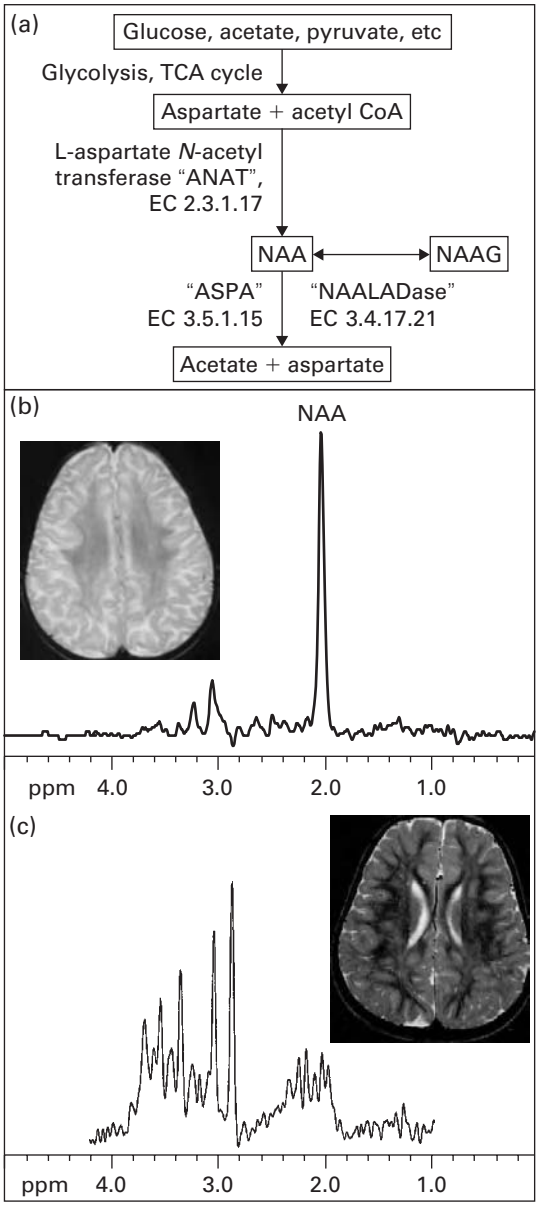

Fig. 1.2 (a) Some biochemical pathways involving NAA, and (b, c) pathological processes involving NAA metabolism. (b) Long TE (270 ms) proton spectra of the frontal WM in a child with Canavan's disease, showing a high ratio of NAA/Cr (and NAA to other metabolites) due to the lack of the enzyme ASPA which degrades NAA. T_2-weighted MRI shows a near complete lack of myelination. (c) A 3-year old boy with mental retardation and complete absence of NAA on brain MRS (short TE). MRI is only mildly abnormal, while other metabolites in the spectrum are also in the normal range. A deficit in the NAA synthetic pathway was suspected, but not proven. Reproduced with permission from Martin *et al.* (2001).

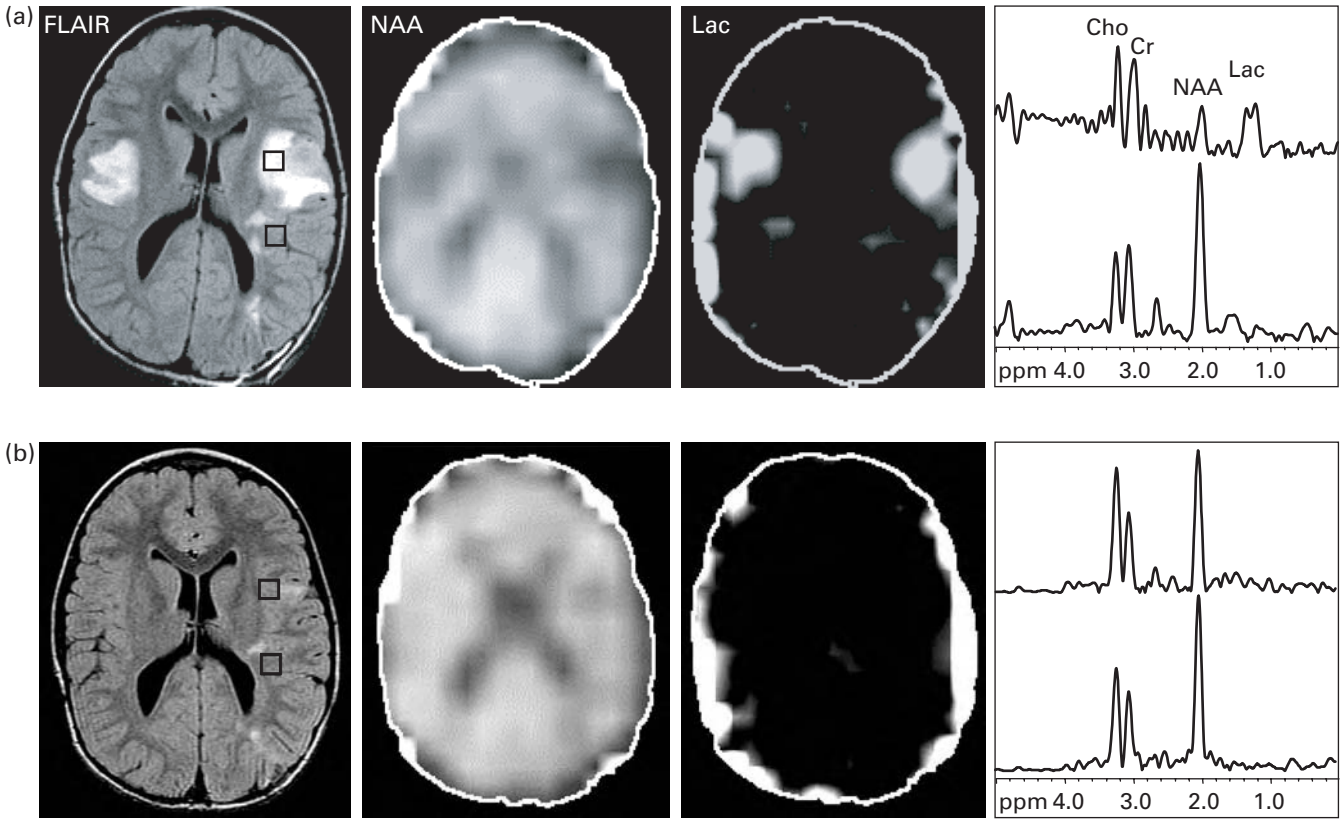

Fig. 1.3 An example of a reversible reduction in NAA in a 6-year old child with ADEM. (a) 36 days after symptom onset, FLAIR MRI shows multiple, bilateral lesions which are characterized by reduced levels of NAA and increased Lac. Cho and Cr are within the normal range. (b) At day 137 after steroid treatment, the lesions have nearly resolved, and the spectra are more normal, in particular NAA has partially recovered and Lac is now undetectable.

In addition, there has been one remarkable case report of a young boy with mental retardation with an apparently global complete absence of NAA (Figure 1.2) (Martin *et al.*, 2001). Clearly, in these subjects, the high levels or absent of NAA do not reflect changes in neuronal density, but rather a perturbation of the synthetic and degradation pathways of NAA metabolism (Figure 1.2). Further examples of the lack of direct correlation of NAA and neuronal density are various pathologies which have shown either spontaneous or treatment-related reversals of NAA decreases. Some examples include MS, mitochondrial diseases, acquired immuno deficiency syndrome (AIDS), temporal lobe epilepsy (TLE), amyotrophic lateral sclerosis (ALS) or acute disseminated encephalomyelitis (ADEM) (Bizzi *et al.*, 2001; Barker, 2001) (Figure 1.3). Evidently, NAA does not appear to be essential for neuronal function.

How should changes (in most instances, decreases) in NAA be interpreted? It should be recognized that the macroscopic concentration of NAA (like that of any neurochemical) depends on the fluxes of synthetic and degradation pathways, cellular density, and brain water content and distribution. Sometimes, a decrease in NAA may be solely or largely attributable simply to increased extracellular water or cerebrospinal fluid (CSF) content within the localized MRS volume, although these factors can be corrected with appropriate analysis techniques (cf. Chapter 2). Neuronal and axonal dysfunction or loss should be considered when the tissue NAA content is reduced, because the balance of evidence suggests that the majority of NAA is located within neuronal processes. Whether the reduction represents an irreversible loss of cells or a potentially reversible

metabolic process will in large part depend on the individual pathology in which it is encountered, and the prognosis for recovery of brain function is presumably also variable. In certain types of lesions (e.g. chronic infarction, brain tumors), it appears likely that in NAA do indeed correspond to irreversible neuronal loss. Overall, non-invasive MRS measurements of NAA appear to be one of the best surrogate markers currently available for neuronal integrity. However, it should be kept in mind that in some pathologies, NAA levels may vary independent of the state of the health and number of neurons.

Choline

The "choline" signal (Cho, 3.24 ppm) arises from the $—N(CH_3)_3$ groups of glycerophosphocholine (GPC), phosphocholine (PC), and a small amount of free Cho, compounds which are involved in membrane synthesis and degradation. Both increases and decreases in Cho have been reported in pathological conditions: processes leading to elevation of Cho signal include active demyelination (Davie *et al.*, 1993), resulting from the degradation of myelin phospholipids primarily to GPC, or increased numbers of glial cells (Gill *et al.*, 1989, 1990). Low Cho has been observed in hepatic encephalopathy (Kreis *et al.*, 1992a), and there is also some evidence to suggest that dietary intake of Cho can modulate cerebral Cho levels (Stoll *et al.*, 1995). Elevated Cho levels seem to be a characteristic of many types of neoplasms, including high-grade brain tumors (provided that they are not necrotic), prostate, breast, head and neck, and others.

Creatine

The "creatine" signal (Cr, 3.02 ppm) is a composite peak consisting of Cr and phosphocreatine, compounds which are involved in energy metabolism via the Cr kinase reaction generating ATP. Since Cr is synthesized in liver, chronic liver disease leads to lower cerebral Cr concentration (Ross and Michaelis, 1994a). There is also a rare group of diseases which involve total Cr deficiency in the brain, resulting from either lack of synthesis in the liver (guanidinoacetate methyl transferase (GAMT) deficiency) or defective transport to the brain (Stockler *et al.*, 1994; Cecil *et al.*, 2001; Bizzi *et al.*, 2002). In vitro, glial cells contain a two- to four-fold higher concentration of Cr than do neurons (Urenjak *et al.*, 1993), although curiously white matter (WM) Cr levels are lower than those of gray matter (GM) in the normal brain.

It has been suggested that the sum of Cr and phosphocreatine is relatively constant in the human brain, and for this reason Cr is often used as a reference signal, and it is a common practice for metabolite ratios to be expressed as a ratio relative to Cr. However, with the development of quantitative analysis techniques, it is clear that total Cr is not constant, both in different brain regions and in pathological processes, so the assumption of Cr as an invariate reference signal should be used with caution. Absolute metabolite quantification techniques are discussed in detail in Chapter 2.

Lactate

In normal human brain, lactate (Lac, 1.33 ppm) is below (or at the limit of) detectability in most studies. Any detectable increase in Lac can therefore be considered abnormal, except perhaps in CSF where it may be detectable at a low level in normal subjects with prominent ventricles. Increased Lac is usually the result of deranged energy metabolism, and has been observed in ischemia (both acute (highest) and chronic (Petroff *et al.*, 1992; Barker *et al.*, 1994)), brain tumors (Alger *et al.*, 1990), mitochondrial diseases (Mathews *et al.*, 1993), and other conditions. Small elevations of Lac have also been reported in the visual cortex (VC) during photic stimulation (Prichard *et al.*, 1991), believed to be due to increased non-oxidative glycolysis, but this effect does not appear to be particularly reproducible (Merboldt *et al.*, 1992).

Myo-inositol

At short TEs, additional compounds are detected which are not visible at long TEs, either because of short T_2 relaxation times and/or the dephasing effects of J-coupling (Figure 1.1(c)). One of the largest signals occurs from myo-inositol (mI) at

3.56 ppm. mI is a pentose sugar, which is part of the inositol triphosphate intracellular second messenger system. Levels have been found to be reduced in hepatic encephalopathy (Ross *et al.*, 1994b), and increased in Alzheimer's dementia (Shonk *et al.*, 1995) and demyelinating diseases (Kruse *et al.*, 1993). The exact pathophysiological significance of alterations in mI is uncertain. A leading hypothesis is that elevated mI reflects increased populations of glial cells which are known to express higher levels of this metabolite than neurons (Brand *et al.*, 1993; Flogel *et al.*, 1994); this may be related to differences in mI/Na co-transporter activity which appears to play a key role in astrocyte osmoregulation (Strange *et al.*, 1994). This would explain chronic disturbance in mI both in degenerative and inflammatory disease, and transiently in hypo- and hyper-osmolar states.

Glutamate and glutamine

Glutamate (Glu) and glutamine (Gln) are difficult to separate in proton spectra at 1.5 T (and are often labeled as a composite peak glutamine and glutamate Glx), although some authors have attempted to distinguish them (Kreis *et al.*, 1992b). At very high fields (at 4 T or above), the C4 resonances of Glu and Gln start to become resolved. Increased cerebral Gln has been found in patients with liver failure (hepatic encephalopathy (Ross *et al.*, 1994b), and Reye's syndrome (Kreis *et al.*, 1995a)) as the result of increased blood ammonia levels, which increases Gln synthesis.

Less commonly detected compounds

A survey of the literature reveals some 25 additional compounds that have been assigned in proton spectra of the human brain. Some of these compounds are present in normal circumstances, but because they are very small and/or overlapping peaks it is usually difficult to detect them. Some examples of these include NAAG, aspartate, taurine, scyllo-inositol, betaine, ethanolamine, purine nucleotides, histidine, glucose, and glycogen (van Zijl and Barker, 1997). Other compounds are yet more difficult to detect and require the use of special spectral editing pulses (beyond the scope of the current chapter) to detect; example of these include γ-amino-butyric acid (GABA), glutathione, and certain macromolecules (Rothman *et al.*, 1993; Terpstra *et al.*, 2003).

Under disease conditions, other compounds may become detectable because their concentration is pathologically increased. Examples of compounds that have been detected under pathological conditions include the ketone bodies β-hydroxy-butyrate and acetone (Seymour *et al.*, 1999; Pan *et al.*, 2001), and other compounds such as phenylalanine (Phe) (in phenylketoneuria (PKU) (Kreis *et al.*, 1995b)), galactitol, ribitol, arabitol in "polyol disease" (van der Knaap *et al.*, 1999), succinate, pyruvate, alanine, glycine, and threonine. Finally, exogenous compounds which are able to cross the blood–brain barrier (BBB) may also reach sufficiently high concentrations to be detected by proton MRS. Examples of exogenous compounds, sometimes termed "xenobiotics", include the drug delivery vehicle propan-1,2-diol (Cady *et al.*, 1994), mannitol (used to reduce swelling and edema in neurosurgical procedures and intensive care), ethanol (Meyerhoff *et al.*, 1996), and the health food supplement methylsulfonylmethane (MSM) (Lin *et al.*, 2001).

In order for a compound to be detectable by proton MRS in vivo, a rule of thumb is that its concentration should be 1 mM or greater, and it should be a small, mobile molecule. Hence large and/or membrane-associated molecules will not be detected. The ability to detect and quantify compounds should increase with increasing magnetic field strength; for instance, a recent study of the normal human brain at 7 T was able to detect more than 14 different compounds (Figure 1.4).

Recently, measurements of brain temperature have also been made using the water–NAA chemical shift difference (the water chemical shift has a 0.01 ppm/°C temperature dependence) (Cady *et al.*, 1995).

Technical issues: spatial localization

Single-voxel techniques

Generally, two different approaches are used for proton spectroscopy of the brain: single-voxel methods

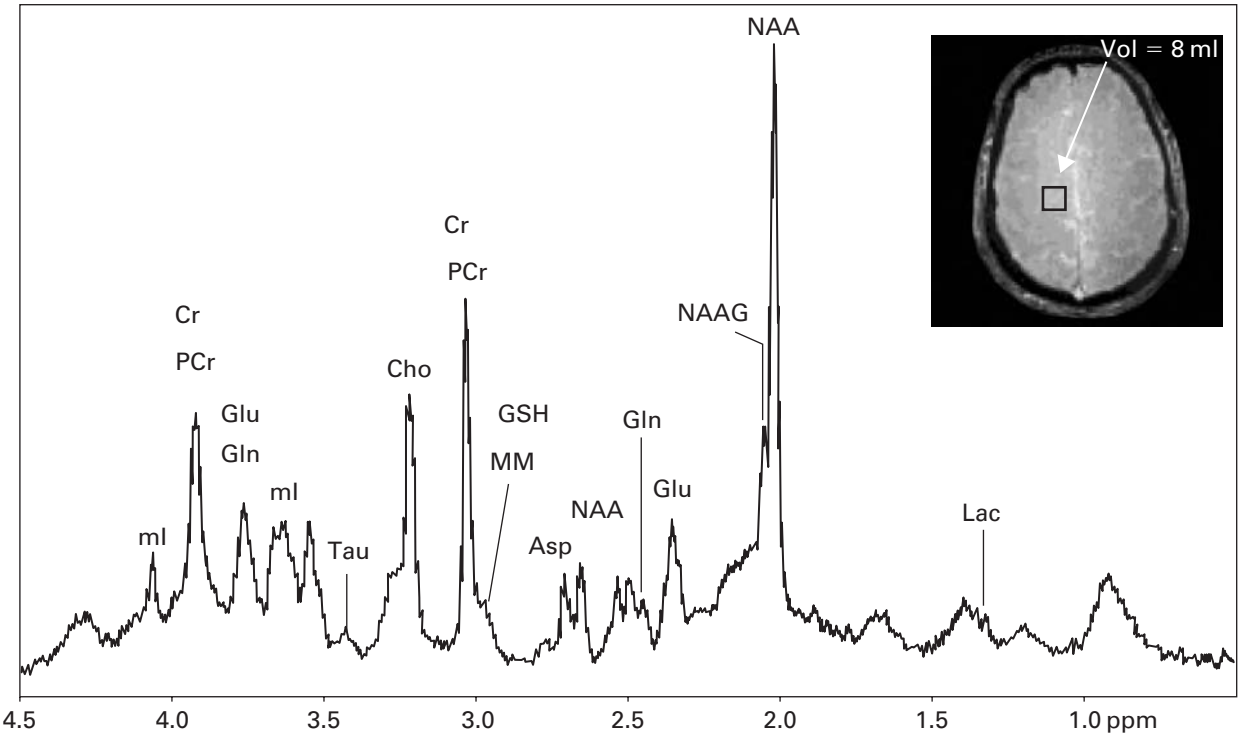

Fig. 1.4 Proton MR spectrum from parietal WM measured at 7 T in the normal human brain. STEAM, TE 56 ms, TM 5 32 ms, TR 5 s, voxel size 5.8 ml, 160 averages (scan time approximately 13 min), resolution enhancement by a shifted Gaussian function. Inset: gradient echo (GE) transverse MRI with the voxel location. Reproduced with permission from Tkac *et al.* (2001).

based on the stimulated echo acquisition mode (STEAM) (Frahm *et al.*, 1989) or point resolved spectroscopy (PRESS) (Bottomley, 1984) pulse sequences, or spectroscopic imaging (SI) (also known as chemical shift imaging (CSI)) studies usually done in two dimensions using a variety of different pulse sequences (spin-echo (SE), PRESS) (Brown *et al.*, 1982; Luyten *et al.*, 1990; Duyn *et al.*, 1993).

The basic principle underlying single-voxel localization techniques is to use (usually) three mutually orthogonal slice selective pulses and design the pulse sequence to collect only the echo signal from the point (voxel) in space where all three slices intersect (Figure 1.5). The two most commonly used sequence are called STEAM (Frahm *et al.*, 1989) and PRESS. In STEAM (Figure 1.5(b)), three 90° pulses are used, and the stimulated echo is collected. All other signals (echoes) should be dephased by the large crusher gradient applied during the so-called mixing time (TM, from analogy with the two-dimensional (2D) NMR nuclear overhauser efffect (NOESY) pulse sequence (Ernst *et al.*, 1987)). Crusher gradients applied during TE on selected gradient channels are necessary for consistent formation of the stimulated echo and removal of unwanted coherences. In PRESS, the second and third pulses are refocusing (180°) pulses, and crusher gradients are applied around these pulses to select the desired SE signal arising from all three RF pulses, and dephasing unwanted coherences. STEAM and PRESS have been the subject of a detailed comparison (Moonen *et al.*, 1989); they are generally similar but differ in a few key respects:

1. *Slice profile (i.e. sharpness of edges of voxel)*: STEAM is somewhat better because it is easier to produce a 90° pulse with a sharp slice profile than a 180° pulse.
2. *SNR*: Provided that equal volumes of tissue are observed and using the same parameters (repetition time (TR), TE, number of averages, etc.),

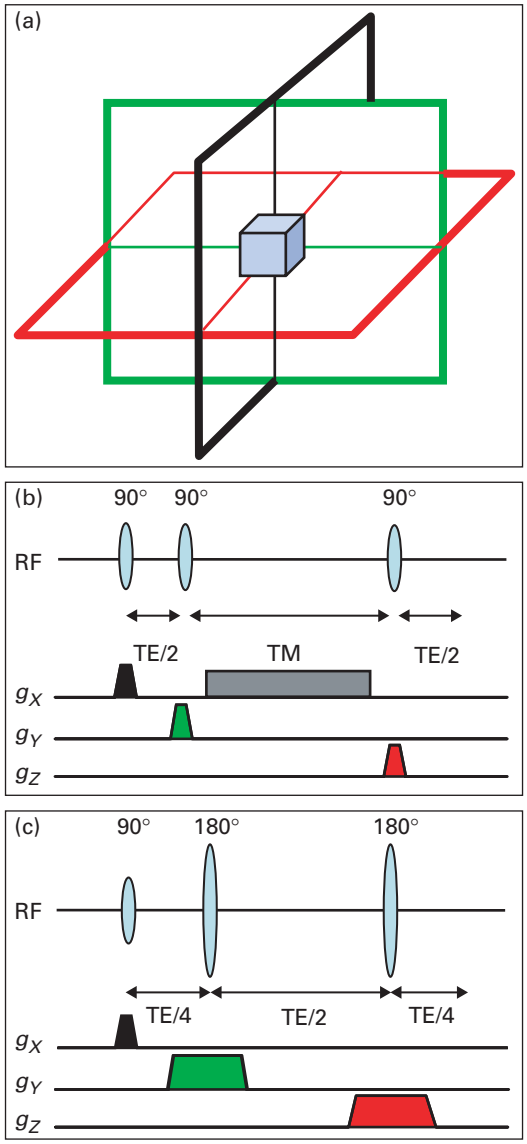

Fig. 1.5 Single-voxel pulse sequences: (a) schematic illustration of three orthogonal slice selective pulses. The size and position of the voxel is controlled by the frequency and bandwidth of the slice selective pulses, as well as by the amplitude of the associated slice selective field gradients, (b) STEAM and (c) PRESS. Note that simplified diagrams are presented which do not show all crusher gradients, gradient lobes and RF pulse shapes.

PRESS should have approximately a factor of two better SNR than STEAM, because the stimulated echo is formed from only half the available equilibrium magnetization.

3. *Minimum TE*: STEAM should have a shorter minimum TE than PRESS, since it uses a TM time period, and shorter 90° than 180° pulses may be possible.
4. *Water suppression*: STEAM may have slightly better water suppression factors, because water suppression (cf. below) pulses can be added during the TM period (this period does not occur in PRESS). Also, STEAM may have less spurious water signal from the 90° slice selective pulses than the 180° pulses in PRESS.
5. *Coupled spin systems and zero-quantum interference*: The complex phenomena that can occur in coupled spin systems (e.g. Lac, Glu, etc.), namely modulation of the echo signal by scalar couplings, and/or the creation of zero- or multiple-quantum coherences, may occur with both sequences. However, the detailed dependence of these compounds' signals on TE and other experimental parameters will be different for STEAM and PRESS. STEAM is more susceptible for the creation of (usually unwanted) zero-quantum coherence because it uses 90° pulses.

It should be recognized that the differences listed above are fairly subtle, and generally STEAM or PRESS are essentially interchangeable in clinical brain spectroscopy, and the choice of sequence in practice often mainly depends on the particular availability from the MRI vendor.

It is important to recognize the importance of accurate spatial localization and suppression of signal from outside the desired voxel. The volume of the human head is two to three orders of magnitude larger than that of the volume of interest (VOI). Even a few percent outer-volume contamination can have a disastrous effect on spectral quality, particularly if field homogeneity is poor in remote regions, and if they contain large water and lipid signals. Methods for maximizing out-of-volume suppression (saturation pulses, optimal use of crusher gradients) are discussed in Chapter 3.

Multiple-voxel (SI) techniques

While single-voxel techniques are popular in clinical practice for several reasons (they have short scan times, are widely available, can be done at short TE, and are relatively easy to use and interpret), they do also suffer some limitations. Probably the greatest

single limitation is the lack of ability to determine spatial heterogeneity of spectral patterns (often very important in brain tumors, for instance), and the fact that only a small number of brain regions can be covered within the time constraints of a normal clinical MR examination.

Therefore, there has been considerable effort over the last decade and a half to develop clinically feasible MR spectroscopic (MRSI) techniques. Early attempts at MRSI in the human brain used one-dimensional (1D)-MRSI (i.e. phase encoding in a single direction) (Petroff *et al.*, 1992), and while these demonstrated proof-of-principle, generally 1D localization is insufficient for detailed studies of focal brain pathology. Therefore, MRSI techniques were extended to two dimensions by using phase-encoding gradients in two directions (Luyten *et al.*, 1990; Duyn *et al.*, 1993) (Figure 1.6), or, subsequently, with full three-dimensional (3D) encoding (Nelson *et al.*, 1999).

One widely used 2D-MRSI pulse sequence combines multi-slice capability with full-slice coverage using a combination of spin-echoes and outer-volume suppression (OVS) pulses (Duyn *et al.*, 1993). The sequence is illustrated schematically in Figure 1.7. Compared to PRESS-MRSI, this sequence can cover the whole slice out to the edge of the cortex, and also record multiple slices. Also, by interleaving multiple slices within one TR, the sequence is very efficient in terms of data collection, and generally, can acquire data at higher spatial resolution and brain coverage than comparable sequences using 3D-MRSI. One potential caveat when attempting wide coverage of brain regions, however, is the difficulty of obtaining sufficient magnetic field homogeneity over the full volume of the brain (simultaneously). For this reason, the sequence of Figure 1.7 is usually performed at long TE (e.g. 140 or 280 ms). These are optimum TEs for detecting the Lac signal (modulation due to scaler coupling causes the Lac signal to be inverted at TE 140 ms). Generally, field homogeneity requirements are less stringent for long TE spectra than short TE, because the spectra are simpler with less overlapping resonances (cf. Chapter 3). Recent technical advances to address this issue include slice-by-slice shimming (i.e. dynamic adjustment of the shim currents within the TR time period for each slice) and the development of high-order shimming in vivo. An excellent approach for localized shimming in vivo is the fast automatic shimming technique by mapping along projections (FASTMAP) method of Gruetter (1993).

An example of a representative multi-slice MRSI data set performed at long TE is given in Figure 1.8. Generally, good quality spectra can be obtained from most parts of the brain, with insufficient field homogeneity only present in regions adjacent to air–tissue interfaces inside the head (e.g. artifacts can be seen in the anterior, mesial temporal lobes and inferior frontal lobe).

MRSI experiments are relatively time consuming, because there are usually a large number of phase-encoding gradient steps to collect. This is particularly true for 2D- or 3D-MRSI experiments that require both high spatial resolution and full (or large) brain coverage. Therefore, there have been various methods proposed to decrease scan time (Duyn and Moonen, 1994; Posse *et al.*, 1995). The discussion of these methods is beyond the scope of this chapter, however increasingly it is expected that fast MRSI techniques will become used for human spectroscopy, such that ultimately MRSI sequences may have similar scan times to single-voxel methods (e.g. 5–10 min, cf. Table 1.2).

Comparison of single-voxel vs. SI techniques

Usually, but not exclusively, single-voxel scans are recorded at short TEs (35 ms) while MRSI studies are done at long TEs (e.g. TE $>$ 135–140 ms). Short TE spectra contain signals from more compounds and have better SNRs, but also have worse water and lipid contamination. Long TE spectra have lower SNR, fewer detectable compounds, and variable amount of T_2-weighting, but are usually better resolved spectra with flatter baselines. Lac is usually best detected at long TEs (e.g. TE = 140 or 280 ms, so that the J-modulation is rephased) to distinguish it from lipid signals. The relative advantages and disadvantages of single-voxel vs. SI techniques are listed in Table 1.1.

The choice of method depends (in addition to availability) on the information required in the particular medical or research application. For instance, if spectroscopy is being used to search for

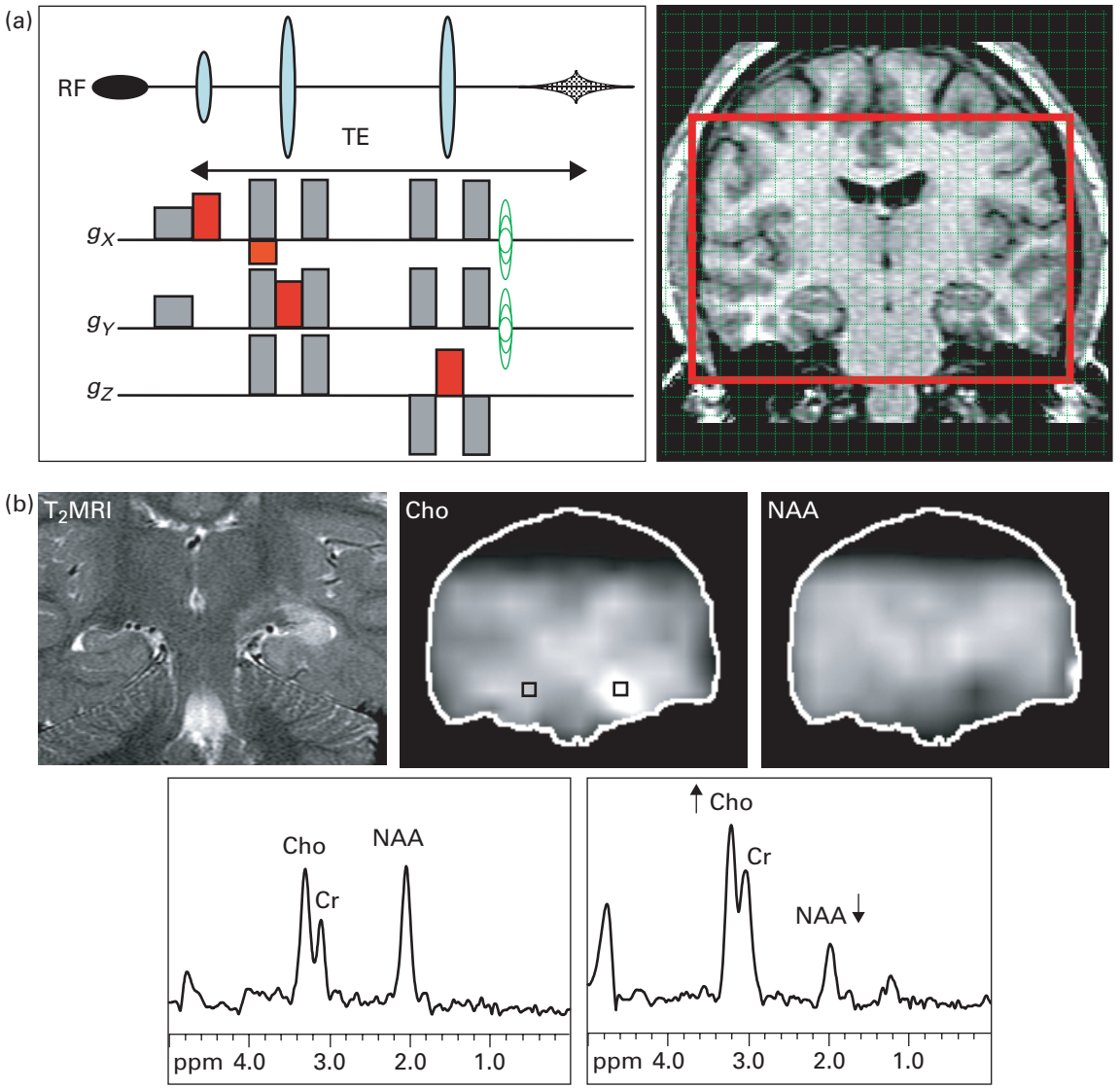

Fig. 1.6 Pulse sequence for 2D PRESS-MRSI. (a) PRESS sequence (red) is used to select a large region of interest (ROI) within the brain (but avoiding unwanted lipid signals in the skull and scalp on this coronal example), and then phase-encoding gradients (green) are applied in two dimensions to encode spatial information inside the excited volume. Data is processed by 3D Fourier transformation (two spatial and one time domains). Full crusher gradients are shown, including those associated with the initial (black) water suppression pulse. Slice selective gradients are indicated in blue. Adapted with permission from (Moonen *et al.*, 1992). (b) An example of the 2D PRESS MRSI pulse sequence in a 14-year old female presenting with seizures with a lesion in the left mesial temporal lobe. Data are presented as metabolic images of NAA and Cho, as well as selected spectra from the left and right hippocampi (voxel positions indicated on Cho images). The lesion has elevated Cho and Cr, and low NAA, typical of a glioma (and atypical for mesial temporal sclerosis which usually shows a selective reduction in NAA only).

the location of a stroke or a seizure focus, SI would be preferable since this generates maps of metabolite levels which can be screened for abnormalities in different locations. Alternatively, if the issue is to observe changes in compounds such as Gln/Glu or mI, which can only be detected in short TE spectra, in global or diffuse diseases such as hepatic encephalopathy, then short TE single-voxel spectroscopy would be the method of choice. Other factors include the length of time available, and whether or not the required voxel location would be better viewed using localized shimming (i.e. single

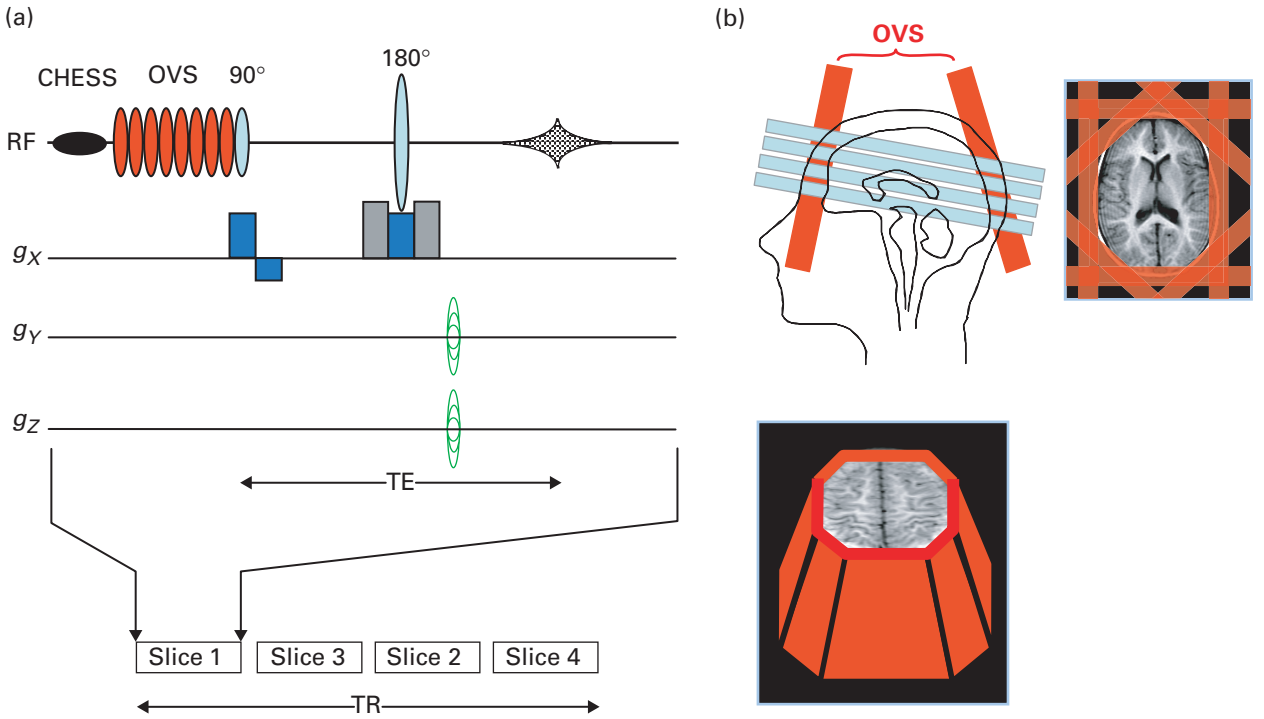

Fig. 1.7 (a) Schematic illustration of pulse sequence for multi-slice MRSI pulse with CHESS water suppression and outer-volume saturation bands for lipid suppression (Duyn *et al.*, 1993) (for clarity, not all crusher gradients are illustrated). A slice selective spin-echo sequence is used, with interleaved acquisition (in this example) or four slices within one TR period. (b) The orientation and locations of the eight OVS pulses are schematically illustrated on sagittal and axial views; an octagonal pattern is prescribed in order to saturated as much peri-cranial lipid as possible while signal from brain is un-perturbed. Ideally, sharp profile, high bandwidth pulses (to minimize chemical shift effects) should be used for OVS.

voxel) or not. Short TE SI is becoming available in commercial sequences and as the techniques become more refined, will provide spatial maps of a greater range of metabolites.

Water and lipid suppression

Brain metabolite levels are on the order of 10 mM or less, whereas protons in brain water are approximately 80 M, and lipids in peri-cranial fat are also present in very high concentrations. Therefore, water and lipid suppression techniques are essential in proton spectroscopy in order to observe reliably the much smaller metabolite signals. Numerous methods for solvent (water) suppression have been developed in high-resolution NMR spectroscopy, and some of these methods have been applied to in vivo spectroscopy. The most common approach is to pre-saturate the water signal using frequency-selective, 90° pulses (chemical shift-selective water suppression (CHESS) pulses (Haase *et al.*, 1985)) prior to localization pulse sequence (Figure 1.7). By using more than one pulse, and with correct choice of flip angles (Moonen and van Zijl, 1990; Ogg, 1994), very good suppression factors can be attained (>1000).

Lipid suppression can be performed in several different ways. One approach is to avoid exciting the lipid signal using, e.g. STEAM or PRESS localization to avoid exciting lipid-containing regions (Figure 1.5). Alternatively (or in addition), OVS pulses can be used to pre-saturate the lipid signal (Duyn *et al.*, 1993) (Figure 1.7). An inversion pulse can also be used for lipid suppression, exploiting the difference in T_1s between lipid (typically 300 ms) and metabolites (typically 1000–2000 ms) (Spielman *et al.*, 1992). Choice of a short inversion time (TI) of around 200 ms ($= T_1 \times \ln[2]$) will selectively null the lipid signal,

Table 1.2. Comparison of single-voxel and multi-voxel MRSI methodologies

	Single voxel	MRSI
TE	Short or long	Usually long, can be short if field homogeneity is good (e.g. small region of coverage)
Typical voxel sizes (cm^3)	4–20	1–4
Typical scan times (min)	5–10	6–30
Shimming	Localized	Global
Water/lipid suppression	Better	Worse
Processing/quantitation	Simple processing, can be quantified	Processing and quantification more time consuming
Multiple voxels	3 or 4 at most	Many voxels

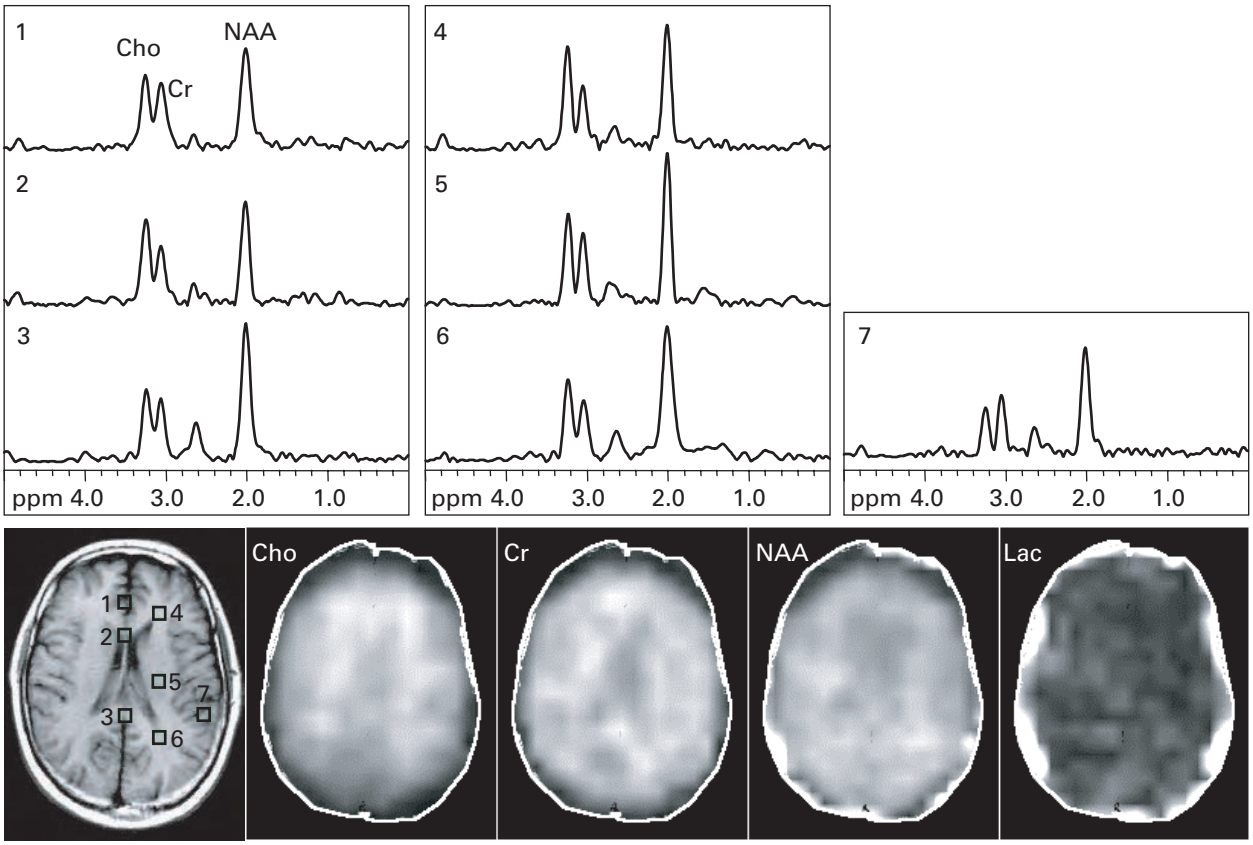

Fig. 1.8 MRSI data recorded using the pulse sequence of Figure 1.7. Metabolic images of Cho, Cr, NAA and lactate from one-slice at the level of the lateral ventricles in a normal 49 year adult are presented, as well as representative spectra from different brain regions. Scan parameters were TR 2300 ms, TE 272 ms, 15 mm slice thickness, field of view (FOV) 24 cm, matrix size 32 × 32, scan time 30 min with circular k-space encoding. The nominal voxel size is 0.8 cm^3. NAA is fairly evenly distributed at this level, while Cho shows an increase from posterior to anterior brain regions (e.g. cf. posterior (6) to anterior (4) WM, and splenium (3) to genu (2) of corpus callosum). Cho is also lower in the lateral GM region (7) compared to WM voxels. No lactate is detectable above the noise floor of the data set.

while most of the metabolite signal remains inverted. In MRSI, it is also possible to reduce lipid artifacts by post-processing methods (Haupt *et al.*, 1996).

Since both water and lipid resonances have shorter T_2 relaxation times than many metabolites, suppression factors are also usually better in long TE compared to short TE spectra.

Data analysis and quantification

Peak area measurements in in vivo spectroscopy are complicated by resonance overlap, baseline distortions, and non-Lorentzian lineshapes. Various methods have been used to measure peak areas, ranging from simple integration to fitting algorithms in the time or frequency domains (Raphael, 1991; de Beer and van Ormondt, 1992). One of the more widely used methods for spectral quantitation in recent years is the linear combination model (LC model) method developed by Provencher *et al*. The LC model fits the in vivo spectrum as a combination of pure, model spectra from each of the expected compounds in the brain (Provencher, 1993). The model also includes automatic phase correction and baseline correction, or the baseline may also be modeled as a combination of macromolecular resonances. Provided that each scanner is properly calibrated with the appropriate model solutions, the program returns metabolite concentrations as well as estimates of uncertainty (e.g. Cramer–Rao lower bounds).

Quantification of in vivo spectra is discussed in detail in Chapter 2. Quantification is important for several reasons, but particularly so in clinical cases where all metabolites (or all regions of the brain) may be abnormal. Quantification methods based on internal or external standards have been extensively developed and tested for single-voxel spectroscopy (Henriksen, 1995) and can be used routinely. With care, it is also possible to quantify MR spectroscopic imaging data (Soher *et al.*, 1996). Occasionally, ratios of peak areas may also be useful, for instance to account for partial volume effects (PVE) or to enhance spectroscopic "contrast" in conditions where metabolites may change in opposite directions (e.g. Cho increases, NAA decreases).

Anatomical variations in brain spectra: changes associated with brain development and aging

Evidently, it is important to establish normal spectral variations associated with age and anatomical location in the healthy control population. Numerous studies have looked at anatomical variations in brain spectra, usually in young adult subjects. At the level of the lateral ventricles and above, brain spectra appear to be fairly homogeneous, with spectra which are characteristic of GM and WM (Kreis *et al.*, 1993a; Michaelis *et al.*, 1993; Hetherington *et al.*, 1994; Soher *et al.*, 1996). Depending on the quantification technique used (and if partial volume correction is applied or not), generally the Cho and NAA signals are found to be marginally higher in WM than cortical GM, with WM showing a lower Cr level than GM. At the level of the third ventricle and below, significant anatomical variations exist in brain spectra. High levels of Cho are found in the insular cortex, and in the region of the hypothalamus. Occipital Cho in the region of the visual cortex is generally low. The pons has high levels of NAA and Cho, and low levels of Cr, perhaps due to its high density of fiber bundles. Cerebellar levels of Cr and Cho are significantly higher than supratentorial values (Michaelis *et al.*, 1993), and temporal lobe has been reported to have lower NAA values (Breiter *et al.*, 1994). Significant anterior–posterior differences have also been reported in normal hippocampal metabolite concentrations, with low NAA and high Cho in the anterior regions of the hippocampus (Vermathen *et al.*, 1997). Relatively fewer papers have addressed the issue of gender differences or metabolic asymmetries in normal brain. However, it appears that there are minimal spectral differences (Charles *et al.*, 1994) with regard to these variables, at least in young adults (Figure 1.9).

Several papers have been published on the changes that occur in proton spectra in the developing brain, and most of the results are in good agreement (van der Knaap *et al.*, 1990; Huppi *et al.*, 1991; Kreis *et al.*, 1993b; Kimura *et al.*, 1995). At birth, NAA is low, while Cho and mI are high, and over the first 1–2 years there is a gradual normalization towards adult values (Figure 1.10) (Kreis *et al.*, 1993b).

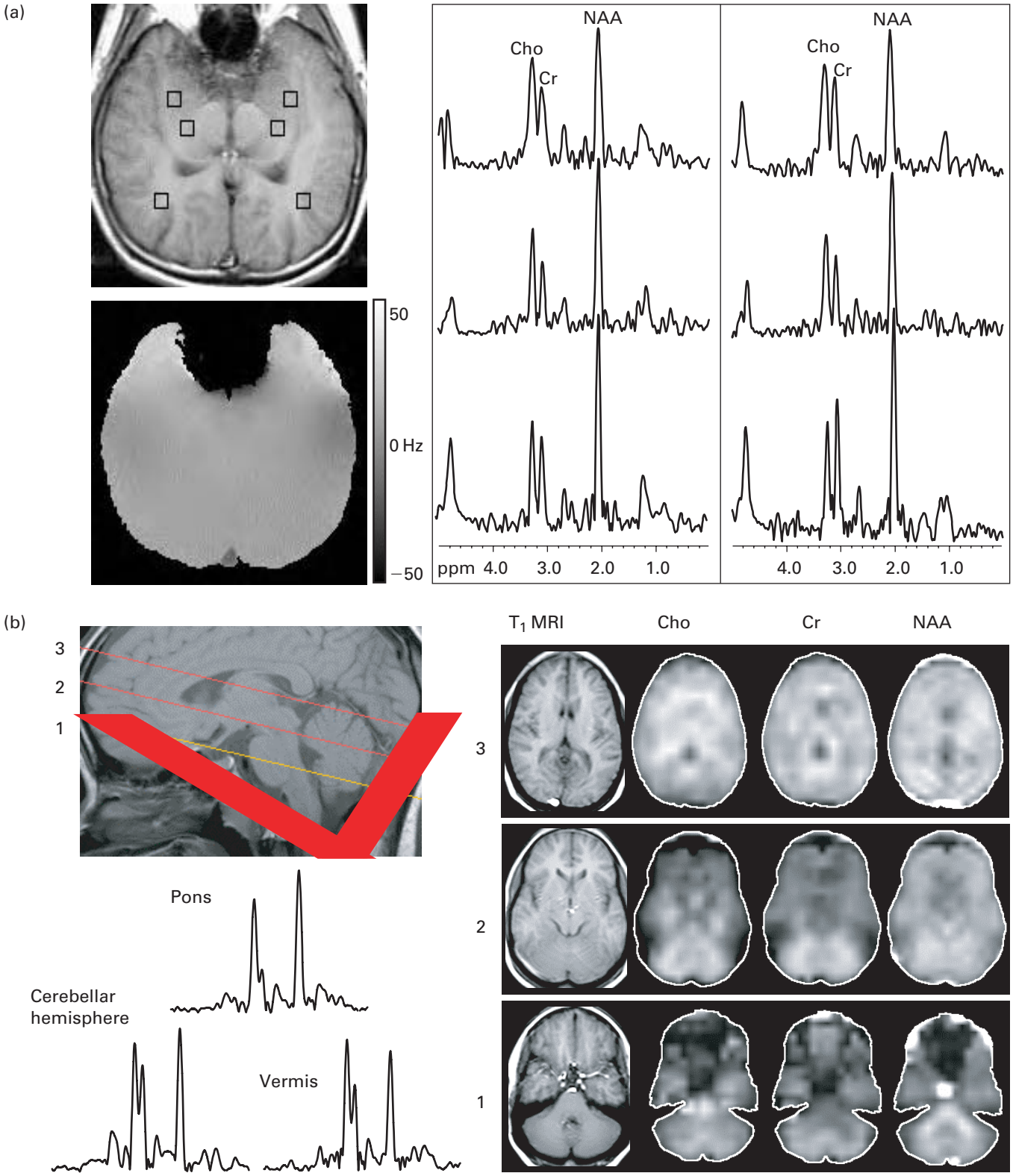

Fig. 1.9 Multi-slice MRSI of (a) temporal lobe and (b) posterior fossa brain regions recorded using the sequence of Figure 1.7. (a) MRSI in an oblique-axial plane parallel to the long axis of the temporal lobe. NAA levels decrease and Cho levels increase in the anterior mesial temporal lobe relative to posterior. Note also the severe field inhomogeneity caused by the sinuses in the frontal region on the B_0 field map. Field homogeneity is also perturbed superior to the auditory canals. (b) MRSI of the posterior fossa. Note the high Cho and Cr levels in the cerebellar vermis and hemispheres. The pons also shows high levels of Cho, but low Cr.

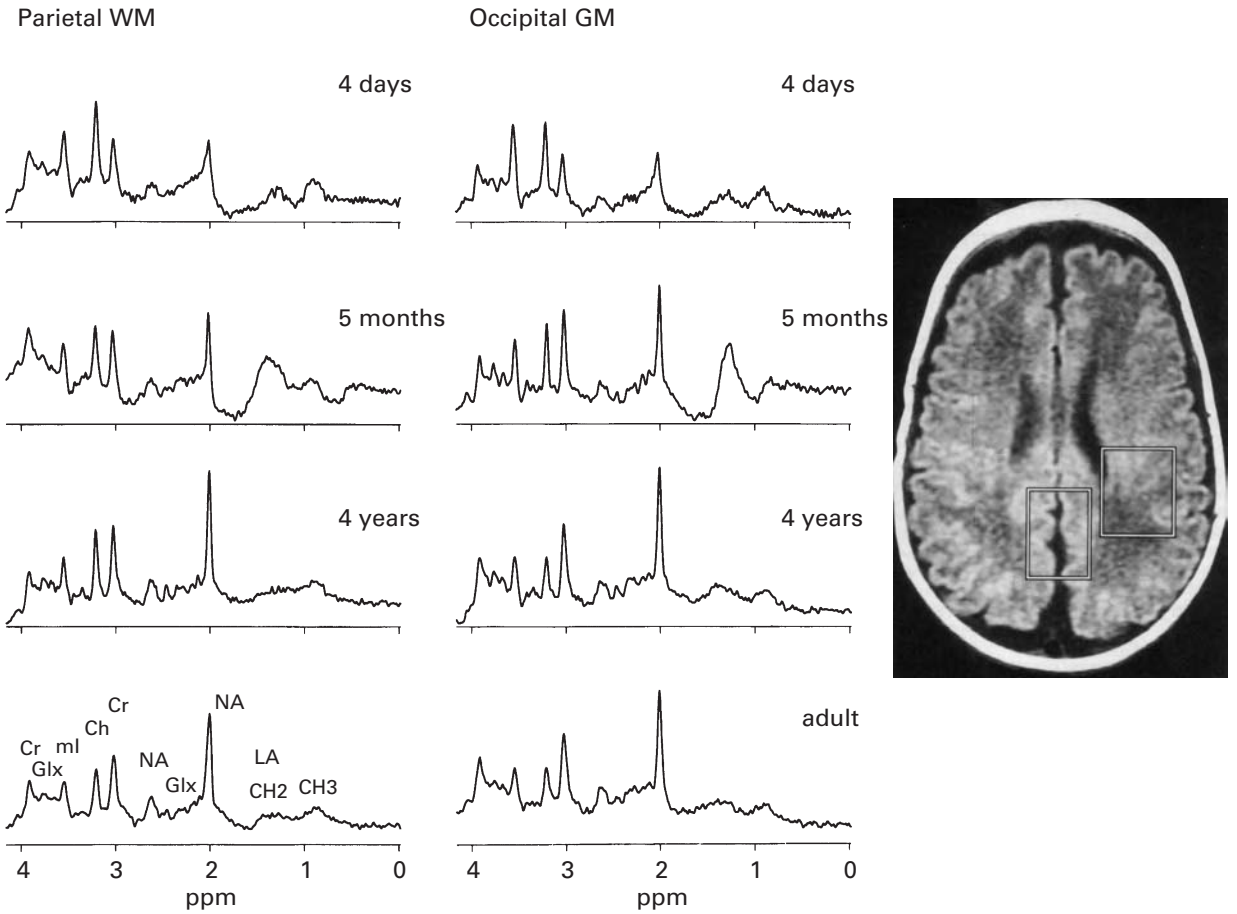

Fig. 1.10 Developmental changes in the human brain. Spectra recorded at short TE (TE 35 ms) are shown in posterior white and GM regions as a function of post-partum age; 4 days, 5 months, 4 years and adult. Note the high levels of Cho and mI at the earliest time point, which decline over the first 2 years of life. Also, NAA is low at birth and increases rapidly. By 4 years of age (in these brain regions), spectra are indistinguishable from those in adults. Reproduced and adapted with permission from (Kreis *et al.*, 1993b).

Similar patterns are seen for both GM and WM, although regional developmental changes have yet to be studied in detail (e.g. using SI). Recent studies have suggested that although the major changes occur within the first year of life, slower changes occur thereafter, with full adult values not being reached until about 20 years of age (Pouwels *et al.*, 1997), and that some regions (e.g. frontal lobe) may develop more slowly than posterior regions (cf. also Chapter 40).

In contrast to studies of developing brain, fewer studies of normal aging have been reported, and the results are less concordant. Some groups find lower NAA with increasing age (Christiansen *et al.*, 1993; Lim and Spielman, 1997), which may reflect neuronal loss, while others find no changes (Chang *et al.*, 1996; Soher *et al.*, 1996). In one study, NAA was only reduced in subjects who also had cerebral atrophy as identified by MRI (Lundbom *et al.*, 1997). Some groups have also found increased levels of Cr or Cho in older subjects, perhaps reflecting increased gliosis (Chang *et al.*, 1996; Soher *et al.*, 1996). This area is discussed further in Chapter 34. The discrepancies between different studies could be due to many different technical factors in data collection and analysis, but may also reflect the wide

physiological variations of normal human aging. More studies are required to definitively establish the spectroscopic characteristics of normal aging, but it is apparent that the changes associated with normal aging are appreciably more subtle than those associated with brain development.

Due to significant technique-related, regional, or age-related changes, it is advisable that spectroscopic studies should have carefully age- and anatomically-matched spectra from control subjects for comparison. In addition, spectroscopic scans of focal brain lesions (for instance) are often much easier to interpret if spectra from normal brain in the contralateral hemisphere are available for comparison.

Summary

Proton MRS and MRSI are now mature methodologies that can be applied routinely on 1.5 T (and higher) imaging systems for the study of neurological disease. The subsequent chapters of this book cover spectral quantification techniques, artifacts and pitfalls, and the clinical applications of these techniques. It is expected that advances in pulse sequence design, analysis methods, and the use of high magnetic fields will continue to occur.

REFERENCES

Alger JR, Frank JA, Bizzi A, Fulham MJ, DeSouza BX, Duhaney MO, Inscoe SW, Black JL, van ZP, Moonen CT, *et al*. 1990. Metabolism of human gliomas: assessment with H-1 MR spectroscopy and F-18 fluorodeoxyglucose PET [see comments]. *Radiology* 177: 633–641.

Arnold DL, Shoubridge EA, Emrich J, Feindel W, Villemure JG. 1989. Early metabolic changes following chemotherapy of human gliomas in vivo demonstrated by phosphorus magnetic resonance spectroscopy. *Invest Radiol* 24: 958–961.

Barker PB, Bryan RN, Kumar AJ, Naidu S. 1992. Proton NMR spectroscopy of Canavan's disease. *Neuropediatrics* 23: 263–267.

Barker PB, Gillard JH, van Zijl PCM, Soher BJ, Hanley DF, Agildere AM, Oppenheimer SM, Bryan RN. 1994. Acute stroke: evaluation with serial proton magnetic resonance spectroscopic imaging. *Radiology* 192.

Barker PB. 2001. *N*-acetyl aspartate – a neuronal marker? *Ann Neurol* 49: 423–424.

Bhakoo KK, Pearce D. 2000. In vitro expression of *N*-acetyl aspartate by oligodendrocytes: implications for proton magnetic resonance spectroscopy signal in vivo. *J Neurochem* 74: 254–262.

Bizzi A, Ulug AM, Crawford TO, Passe T, Bugiani M, Bryan RN, Barker PB. 2001. Quantitative proton MR spectroscopic imaging in acute disseminated encephalomyelitis. *Am J Neuroradiol* 22: 1125–1130.

Bizzi A, Bugiani M, Salomons GS, Hunneman DH, Moroni I, Estienne M, Danesi U, Jakobs C, Uziel G. 2002. X-linked creatine deficiency syndrome: a novel mutation in creatine transporter gene SLC6A8. *Ann Neurol* 52: 227–231.

Bloch F. 1946. Nuclear induction. *Phys Rev* 70: 460–474.

Bottomley P. 1984. In *U.S. Patent,* Vol. 4 480 228 USA.

Breiter SN, Arroyo S, Mathews VP, Lesser RP, Bryan RN, Barker PB. 1994. Proton magnetic resonance spectroscopy in patients with seizure disorders. *Am J Neuroradiol* 15: 373–384.

Brand A, Richter-Landsberg C, Leibfritz D. 1993. Multinuclear NMR studies on the energy metabolism of glial and neuronal cells. *Dev Neurosci* 15(305): 289–298.

Brown T, Kincaid B, Ugurbil K. 1982. NMR Chemical shift imaging in three dimensions. *Proc Natl Acad Sci* USA, 79: 3523–3526.

Burlina AP, Ferrari V, Facci L, Skaper SD, Burlina AB. 1997. Mast cells contain large quantities of secretagogue-sensitive *N*-acetylaspartate. *J Neurochem* 69: 1314–1317.

Cadoux HT, Blackledge MJ, Rajagopalan B, Taylor DJ, Radda GK. 1989. Human primary brain tumour metabolism in vivo: a phosphorus magnetic resonance spectroscopy study. *Br J Cancer* 60: 430–436.

Cady EB, Lorek A, Penrice J, Reynolds EO, Iles RA, Burns SP, Coutts GA, Cowan FM. 1994. Detection of propan-1,2-diol in neonatal brain by in vivo proton magnetic resonance spectroscopy. *Magn Reson Med* 32: 764–767.

Cady EB, D'Souza PC, Penrice J, Lorek A. 1995. The estimation of local brain temperature by in vivo 1H magnetic resonance spectroscopy. *Magn Reson Med* 33: 862–867.

Cecil KM, Salomons GS, Ball Jr WS, Wong B, Chuck G, Verhoeven NM, Jakobs C, DeGrauw, TJ. 2001. Irreversible brain creatine deficiency with elevated serum and urine creatine: a creatine transporter defect? *Ann Neurol* 49: 401–404.

Chang L, Ernst T, Poland RE, Jenden DJ. 1996. In vivo proton magnetic resonance spectroscopy of the normal aging human brain. *Life Sci* 58: 2049.

Charles HC, Lazeyras F, Krishnan KRR, Boyko OB, Patterson LJ, Doraiswamy PM, McDonald WM. 1994. Proton spectroscopy of human brain: effects of age and sex. *Prog Neuro-Psychopharmacol and Biol Psychiat* 18: 995.

Christiansen P, Toft P, Larsson HBW, Stubgaard M, Henriksen O. 1993. The concentration of *N*-acetyl aspartate, creatine + phosphocreatine, and choline in different parts of the brain in adulthood and senium. *Magn Reson Imaging* 11: 799.

Davie CA, Hawkins CP, Barker GJ, Brennan A, Tofts PS, Miller DH, McDonald WI. 1993. Detection of myelin breakdown products by proton magnetic resonance spectroscopy. *Lancet* 341: 630–631.

de Beer R, van Ormondt D. 1992. In *NMR Basic Principles and Progress*, Vol. 26 (Eds., Diehl P, Fluck E, Günther H, Kosfeld R, Seelig J, Rudin M), Springer-Verlag, Berlin, pp. 201–248.

De Stefano N, Narayanan S, Francis GS, Arnaoutelis R, Tartaglia MC, Antel JP, Matthews PM, Arnold DL. 2001. Evidence of axonal damage in the early stages of multiple sclerosis and its relevance to disability. *Arch Neurol* 58: 65–70.

Duyn JH, Gillen J, Sobering G, van Zijl PCM, Moonen CTW. 1993. Multislice proton MR spectroscopic imaging of the brain. *Radiology* 188: 277–2 82 .

Duyn JH, Moonen CTW. 1994. Fast proton spectroscopic imaging of the human brain using multiple spin-echoes. *Magn Reson Med* 30: 409–414.

Ernst R, Bodenhausen G, Wokaun A. 1987. *Principles of Nuclear Magnetic Resonance in One and Two Dimensions*, Oxford University Press, Oxford.

Flogel U, Willker W, Leibfritz D. 1994. Regulation of intracellular pH in neuronal and glial tumour cells, studied by multinuclear NMR spectroscopy. *NMR Biomed* 7: 157–166.

Frahm J, Bruhn H, Gyngell ML, Merboldt KD, Hanicke W, Sauter R. 1989. Localized high-resolution proton NMR spectroscopy using stimulated echoes: initial applications to human brain in vivo. *Magn Reson Med* 9: 79–93.

Frahm J, Michaelis T, Merboldt K.-D, Hanicke W, Gyngell ML, Bruhn H. 1991. On the *N*-acetyl methyl resonance in localized 1H NMR spectra of the human brain in vivo. *NMR Biomed* 4: 201–204.

Gill SS, Small RK, Thomas DG, Patel P, Porteous R, van Bruggen N, Gadian DG, Kauppinen RA, Williams SR. 1989. Brain metabolites as 1H NMR markers of neuronal and glial disorders. *NMR Biomed* 2: 196–200.

Gill SS, Thomas DG, Van BN, Gadian DG, Peden CJ, Bell JD, Cox IJ, Menon DK, Iles RA, Bryant DJ. 1990. Proton MR spectroscopy of intracranial tumours: in vivo and in vitro studies. *J Comput Assist Tomogr* 14: 497–504.

Gruetter R. 1993. Automatic, localized in vivo adjustment of all first- and second-order shim coils. *Magn Reson Med* 29: 804–811.

Guimaraes A, Schwartz P, Prakash MR, Carr CA, Berger UV, Jenkins BG, Coyle JT, Gonzalez RG. 1995. Quantitative in vivo 1H nuclear magnetic resonance spectroscopic imaging of neuronal loss in rat brain. *Neuroscience* 69: 1095.

Gutowsky HS, McCall DW, Slichter CP. 1951. *Phys Rev* 84: 589.

Haase A, Frahm J, Hanicke W, Matthei D. 1985. ^{1}H NMR chemical shift selective imaging. *Phys Med Biol* 30: 341–344.

Haupt CI, Schuff N, Weiner MW, Maudsley AA. 1996. Removal of lipid artifacts in 1H spectroscopic imaging by data extrapolation. *Magn Reson Med* 35: 678–687.

Henriksen O. 1995. In vivo quantitation of metabolite concentrations in the brain by means of proton MRS. *NMR Biomed* 8: 139–148.

Hetherington HP, Mason GF, Pan JW, Ponder SL, Vaughan JT, Twieg DB, Pohost GM. 1994. Evaluation of cerebral gray and white matter metabolite differences by spectroscopic imaging at 4.1T. *Magn Reson Med* 32: 565–571.

Huppi PS, Posse S, Lazeyras F, Burri R, Bossi E, Herschkowitz N. 1991. Magnetic resonance in preterm and term newborns: 1H-spectrscopy in developing brain. *Pediatric Res* 30: 574–578.

Kimura H, Fujii Y, Itoh S, Matsuda T, Iwasaki T, Maeda M, Konishi Y, Ishii Y. 1995. Metabolic Alterations in the neonate and infant brain during development: evaluation with proton MR spectroscopy. *Radiology* 194: 483–489.

Kreis R, Ross BD, Farrow NA, Ackerman Z. 1992a. Metabolic disorders of the brain in chronic hepatic encephalopathy detected with H-1 MR spectroscopy. *Radiology* 182: 19–27.

Kreis R, Ross BD, Farrow NA, Ackerman Z. 1992b. Metabolic disorders of the brain in chronic hepatic encephalopathy detected with H-1 MR spectroscopy. *Radiology* 182: 19–27.

Kreis R, Ernst T, Ross B. 1993a. Absolute quantitation of water and metabolites in the human brain. II metabolite concentrations. *J Magn Reson B* 102: 9–19.

Kreis R, Ernst T, Ross BD. 1993b. Development of the human brain: In vivo quantification of metabolite and water content with proton magnetic resonance spectroscopy. *Magn Reson Med* 30: 424–437.

Kreis R, Pfenninger J, Herschkowitz N, Boesch C. 1995a. In vivo proton magnetic resonance spectroscopy in a case of Reye's syndrome. *Intens Care Med* 21: 266–269.

Kreis R, Pietz J, Penzien J, Herschkowitz N, Boesch C. 1995b. Identification and quantitation of phenylalanine in the brain of patients with phenylketonuria by means of localized in vivo 1H magnetic-resonance spectroscopy. *J Magn Reson B* 107: 242–251.

Kruse B, Hanefeld F, Christen HJ, Bruhn H, Michaelis T, Hanicke W, Frahm J. 1993. Alterations of brain metabolites in metachromatic leukodystrophy as detected by localized proton magnetic resonance spectroscopy in vivo. *J Neurol* 241: 68–74.

Levine SR, Helpern JA, Welch KM, Vande LA, Sawaya KL, Brown EE, Ramadan NM, Deveshwar RK, Ordidge RJ. 1992.

Human focal cerebral ischemia: evaluation of brain pH and energy metabolism with P-31 NMR spectroscopy. *Radiology* 185: 537–544.

Lim KO, Spielman DM. 1997. Estimating NAA in cortical gray matter with applications for measuring changes due to aging. *Magn Reson Med* 37: 372–377.

Lin A, Nguy CH, Shic F, Ross BD. 2001. Accumulation of methylsulfonylmethane in the human brain: identification by multinuclear magnetic resonance spectroscopy. *Toxicol Lett* 123: 169–177.

Lundbom N, Barnett A, Bonavita S, Patronas N, Rajapakse J, Tedeschi G, Di Chiro G. 1997. In *ISMRM 5th Scientific Meeting and Symposium*, Vancouver, BC, pp. 1209.

Luyten PR, Groen JP, Vermeulen JW, den HJ. 1989. Experimental approaches to image localized human 31P NMR spectroscopy. *Magn Reson Med* 11: 1–21.

Luyten PR, Marien AJ, Heindel W, van GP, Herholz K, den HJ, Friedmann G, Heiss WD. 1990. Metabolic imaging of patients with intracranial tumors: H-1 MR spectroscopic imaging and PET. *Radiology* 176: 791–799.

Martin E, Capone A, Schneider J, Hennig J, Thiel T. 2001. Absence of *N*-acetylaspartate in the human brain: impact on neurospectroscopy? *Ann Neurol* 49: 518–521.

Mathews PM, Andermann F, Silver K, Karpati G, Arnold DL. 1993. Proton MR spectroscopic characterization of differences in regional brain metabolic abnormalities in mitochondrial encephalomyopathies. *Neurology* 43: 2484–2490.

Merboldt K-D, Bruhn H, Hanicke W, Michaelis T, Frahm J. 1992. Decrease of glucose in the human visual cortex during photic stimulation. *Magn Reson Med* 25: 187–194.

Meyerhoff DJ, Rooney WD, Tokumitsu T, Weiner MW. 1996. Evidence of multiple ethanol pools in the brain: an in vivo proton magnetization transfer study. *Alcohol Clin Exp Res* 20: 1283–1288.

Michaelis T, Merboldt K-D, Bruhn H, Hanicke W, Frahm J. 1993. Absolute concentrations of metabolites in the adult human brain in vivo: quantification of localized proton MR spectra. *Radiology* 187: 219–227.

Moonen CT, van Zijl PCM, Gillen J, Daly P, von Kienlin M, Wolf J, Cohen J. 1989. Comparison of single-shot localization methods (STEAM and PRESS) for in vivo proton NMR spectroscopy. *NMR Biomed* 2: 201–208.

Moonen CTW, van Zijl, PCM. 1990. Highly efficient water suppression for in vivo proton NMR spectroscopy. *J Magn Reson* 88: 28–41.

Moonen CTW, Sobering G, van Zijl PCM, Gillen J, von Kienlin M, Bizzi A. 1992. Proton spectroscopic imaging of human brain. *J Magn Reson* 98: 556–575.

Nelson SJ, Vigneron DB, Dillon WP. 1999. Serial evaluation of patients with brain tumors using volume MRI and 3D 1H MRSI. *NMR Biomed* 12: 123–138.

Ogg RJ, Kingsley PB, Taylor JS. 1994. WET, a T_1 and B_1-insensitive water suppression method for in vivo localized ^{1}H NMR spectroscopy. *J Magn Reson* B104: 1–10.

Pan JW, Telang FW, Lee JH, de Graaf RA, Rothman DL, Stein DT, Hetherington HP. 2001. Measurement of beta-hydroxybutyrate in acute hyperketonemia in human brain. *J Neurochem* 79: 539–544.

Petroff OAC, Graham GD, Blamire AM, al Rayess M, Rothman DL, Fayad PB, Brass LM, Shulman RG, Prichard JW. 1992. Spectroscopic imaging of stroke in humans: histopathology correlates of spectral changes. *Neurology* 42: 1349–1354.

Posse S, Tedeschi G, Risinger R, Ogg R, Le Bihan D. 1995. High speed 1H spectroscopic imaging in human brain by echo planar spatial-spectral encoding. *Magn Reson Med* 33: 34–40.

Pouwels PJW, Kruse B, Hanefeld F, Frahm J. 1997. In *ISMRM 5th Scientific Meeting and Exhibition*, Vancouver, BC, pp. 482.

Prichard J, Rothman D, Novotny E, Petroff O, Kuwabara T, Avison M, Howseman A, Hanstock C, Shulman R. 1991. Lactate rise detected by 1H NMR in human visual cortex during physiologic stimulation. *Proc Natl Acad Sci USA* 88: 5829–5831.

Proctor WG, Yu FC. 1950. The dependence of a nuclear magnetic resonance frequency upon chemical compound. *Phys Rev* 77: 717.

Provencher SW. 1993. Estimation of metabolite concentrations from localized in vivo proton NMR spectra. *Magn Reson Med* 30: 672–679.

Purcell EU, Torrey HC, Pound RV. 1946. Resonance absorption by nuclear magnetic moments in a solid. *Phys Rev* 69: 37–38.

Radda GK. 1986. The use of NMR spectroscopy for the understanding of disease. *Science* 233: 640–655.

Raphael C. 1991. In vivo NMR spectral parameter estimation: a comparison between time and frequency domain methods. *Magn Reson Med* 18: 358–370.

Ross BD, Michaelis T. 1994a. Clinical applications of magnetic resonance spectroscopy. *Magn Reson Q* 10: 191–247.

Ross BD, Jacobson S, Villamil F, Korula J, Kreis R, Ernst T, Shonk T, Moats RA. 1994b. Subclinical hepatic encephalopathy: proton MR spectroscopic abnormalities. *Radiology* 193: 457–463.

Rothman DL, Petroff OA, Behar KL, Mattson RH. 1993. Localized 1H NMR measurements of gamma-aminobutyric acid in human brain in vivo. *Proc Natl Acad Sci USA* 90: 5662–5666.

Seymour KJ, Bluml S, Sutherling J, Sutherling W, Ross BD. 1999. Identification of cerebral acetone by 1H-MRS in patients with epilepsy controlled by ketogenic diet. *Magma* 8: 33–42.

Shonk TK, Moats RA, Gifford P, Michaelis T, Mandigo JC, Izumi J, Ross BD. 1995. Probable Alzheimer disease: diagnosis with proton MR spectroscopy [see comments]. *Radiology* 195: 65–75.

Simmons ML, Frondoza CG, Coyle JT. 1991. Immunocytochemical localization of N-acetyl-aspartate with monoclonal antibodies. *Neuroscience* 45: 37–45.

Soher BJ, van Zijl PCM, Duyn JH, Barker PB. 1996. Quantitative proton spectroscopic imaging of the human brain. *Magn Reson Med* 35: 356–363.

Spielman DM, Pauly JM, Macovski A, Glover GH, Enzmann DR. 1992. Lipid-suppressed single- and multisection proton spectroscopic imaging of the human brain. *J Magn Reson Imaging* 2: 253–262.

Stockler S, Holzbach U, Hanefeld F, Marquardt I, Helms G, Requart M, Hanicke W, Frahm J. 1994. Creatine deficiency in the brain: a new, treatable inborn error of metabolism. *Pediatr Res* 36: 409–13.

Stoll AL, Renshaw PF, De Micheli E, Wurtman R, Pillay SS, Cohen BM. 1995. Choline ingestion increases the resonance of choline-containing compounds in human brain: an in vivo proton magnetic resonance study. *Biol Psychiatry* 37: 170–174.

Strange K, Emma F, Paredes A, Morrison R. 1994. Osmoregulatory changes in myo-inositol content and Na+/Myo-inositol cotransport in rat cortical astrocytes. *Glia* 12(1): 35–43.

Terpstra M, Henry PG, Gruetter R. 2003. Measurement of reduced glutathione (GSH) in human brain using LC model analysis of difference-edited spectra. *Magn Reson Med* 50: 19–23.

Tkac I, Andersen P, Adriany G, Merkle H, Ugurbil K, Gruetter R. 2001. In vivo 1H NMR spectroscopy of the human brain at 7T. *Magn Reson Med* 46: 451–456.

Urenjak J, Williams SR, Gadian DG, Noble M. 1992. Specific expression of *N*-acetylaspartate in neurons, oligodendrocyte- type-2 astrocyte progenitors, and immature oligodendrocytes in vitro. *J Neurochem* 59: 55–61.

Urenjak J, Williams SR, Gadian DG, Noble M. 1993. Proton nuclear magnetic resonance spectroscopy unambiguously identifies different neural cell types. *J Neurosc* 13: 981.

van der Knaap MS, van der Grond J, van Rijen PC, Faber JAJ, Valk J, Willemse K. 1990. Age-dependent changes in localized proton and phosphorus MR spectrscopy of the brain. *Radiology* 176: 509–515.

van der Knaap MS, Wevers RA, Struys EA, Verhoeven NM, Pouwels PJ, Engelke UF, Feikema W, Valk J, Jakobs C. 1999. Leukoencephalopathy associated with a disturbance in the metabolism of polyols. *Ann Neurol* 46: 925–928.

van Zijl PCM, Barker PB. 1997. In *Imaging Brain Structure and Function*, Vol. 820, New York, NY, pp. 75–96.

Vermathen P, Laxer KD, El Din M, Matson GB, Weiner MW. 1997. In *ISMRM 5th Scientific Meeting and Symposium,* Vancouver, BC, pp. 36.

2

Quantification and analysis in MR spectroscopy

Thomas Ernst

Department of Medicine, University of Hawaii, John A. Burns School of Medicine, Honolulu, Hawaii

Key points

- Spectral quantification allows detection of metabolite abnormalities that are not appreciated from visual inspection alone.
- Metabolite ratio determination is robust and reproducible in a clinical environment, but prone to changes in the denominator metabolite concentration (commonly creatine).
- Spectra may be fitted in the time or frequency domain.
- Absolute metabolite quantification requires internal or external reference standards, and correction for tissue volumes (e.g. cerebrospinal fluid) within the voxel. Water is a commonly used internal reference signal.
- Chemical shift imaging allows calculation of metabolite levels within different tissues, e.g. gray and white matter.

Introduction

Why quantification and not visual interpretation?

The quantification of spectral peaks plays an important role in MR spectroscopy (MRS), and pure visual readings of spectra are less common compared to MR imaging (MRI). The reason for this difference is that MRI relies on the detection of spatial or signal abnormalities as a result of disease conditions, whereas MRS interpretation commonly relies on the interpretation of differences in relative proportions of metabolite peaks at a given location. Furthermore, spectroscopic peaks reflect the concentrations of metabolites in the tissue; however, it is impossible to determine these concentrations visually.

These points are illustrated in Figure 2.1, which shows proton spectra from a lymphoma lesion and a contralateral voxel in a patient with acquired immuno deficiency syndrome (AIDS). Since the spectra can be plotted with arbitrary vertical scaling, it is unclear if a given metabolite peak, and its associated concentration, in the lesion is higher or lower compared to the healthy brain tissue. It is even difficult to estimate the relative heights of the metabolite peaks within each voxel. Therefore, the ultimate goal of spectral analysis is to determine accurate estimates of metabolite peak areas that reflect metabolite concentrations.

Spectral analysis

Overview

The first major step in determining metabolite concentrations is to obtain the signal strength S_m of each metabolite in a given spectrum. Typically, sophisticated computer algorithms are used for this purpose. We will describe the major techniques and discuss major advantages and problems. However, the exact details of the analysis often will be completely hidden from the user, especially with some of the more recent automated programs, and most likely will have only minor influence on the quality of the analyses.

Spectral analysis can be performed in the "time domain", using the so-called "free-induction decay"

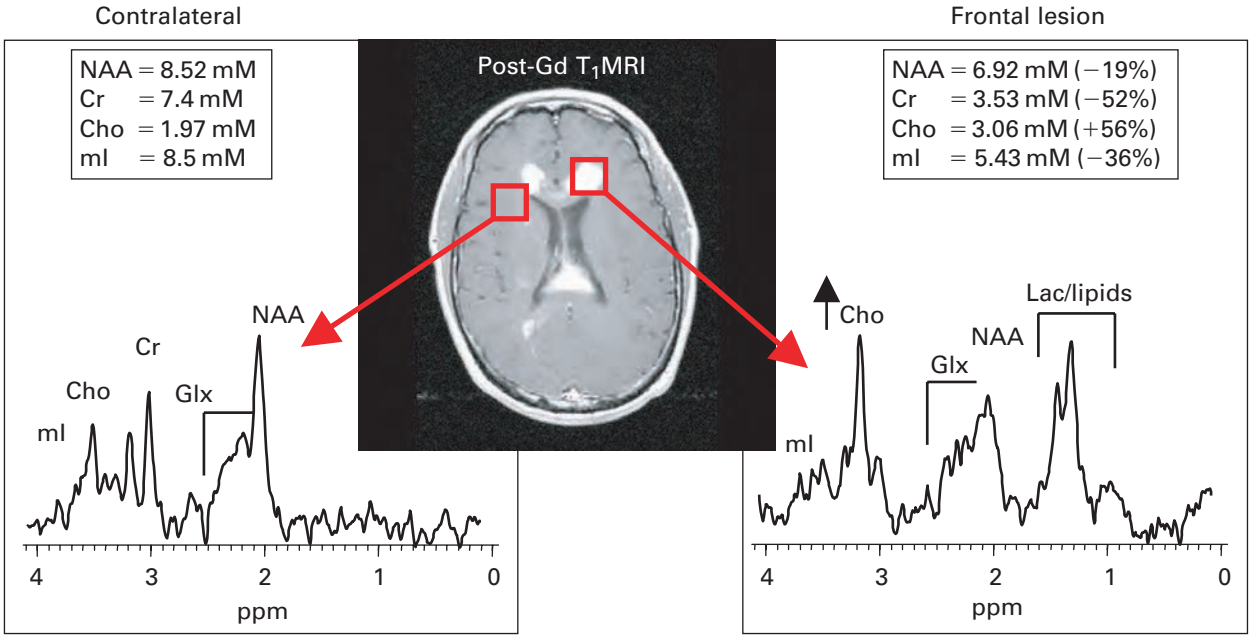

Fig. 2.1 Localized ^{1}H MR spectra from a lymphoma in the left frontal lobe and from a contralateral control region in normal-appearing white matter (WM). While visual inspection shows clear differences between the two spectra, it does not allow an accurate, quantitative assessment of the metabolite abnormalities. Spectral quantification, using the water signal as a reference, makes it possible to calculate millimolar (mM) metabolite concentrations, and demonstrates that the lymphoma lesion has reduced concentrations of *N*-acetyl aspartate (NAA) compounds, total creatine (Cr), and myo-inositol (mI), whereas the concentration of Choline (Cho) compounds is increased in the lesion. Glx, glutamate (Glu) + glutamine (Gln).

(or FID), or the "frequency domain", using "spectra" after Fourier transformation of the time-domain data. Of these two, analysis in the frequency domain (Mierisova and Ala-Korpela, 2001), i.e. the use of spectra, is more intuitive and will be discussed first. The steps involved in frequency-domain spectral analysis are exemplified in Figure 2.2 and outlined below. Historically, the steps were performed sequentially and manually by a spectroscopist; however, more recent spectral analysis programs are completely automatic.

Time domain pre-processing

Spectral analysis typically involves several pre-processing steps in the time domain that are summarized in Figure 2.2 (top row). First, the digital time domain spectral data (FIDs) are corrected to remove phase variations due to residual gradient-induced eddy currents (Klose, 1990; Lin *et al.*, 1994). Next, a digital filter is commonly applied that removes the potentially very large residual water signal (Coron *et al.*, 2001). The resulting data are multiplied with a decaying function, such as a decaying exponential, to artenuate signals on the right side of the FID. This step is called "low-pass filtering" or "apodization," and reduces noise in the spectrum (cf. Figure 2.2), but at the expense of increasing spectral linewidths. Finally, the apodized are padded with zeroes on the right side (cf. Figure 2.2); for instance, the total number of data points may be increased from 1024 to 2048 or 4096. This step is called "zero-filling" and improves the digital resolution of spectra.

Fourier transformation

The zero-filled, low-pass filtered, and eddy-current corrected time-domain data are then Fourier transformed, which yields frequency-domain data (spectra). The remaining processing steps are applied in the frequency domain (cf. Figure 2.2, bottom row).

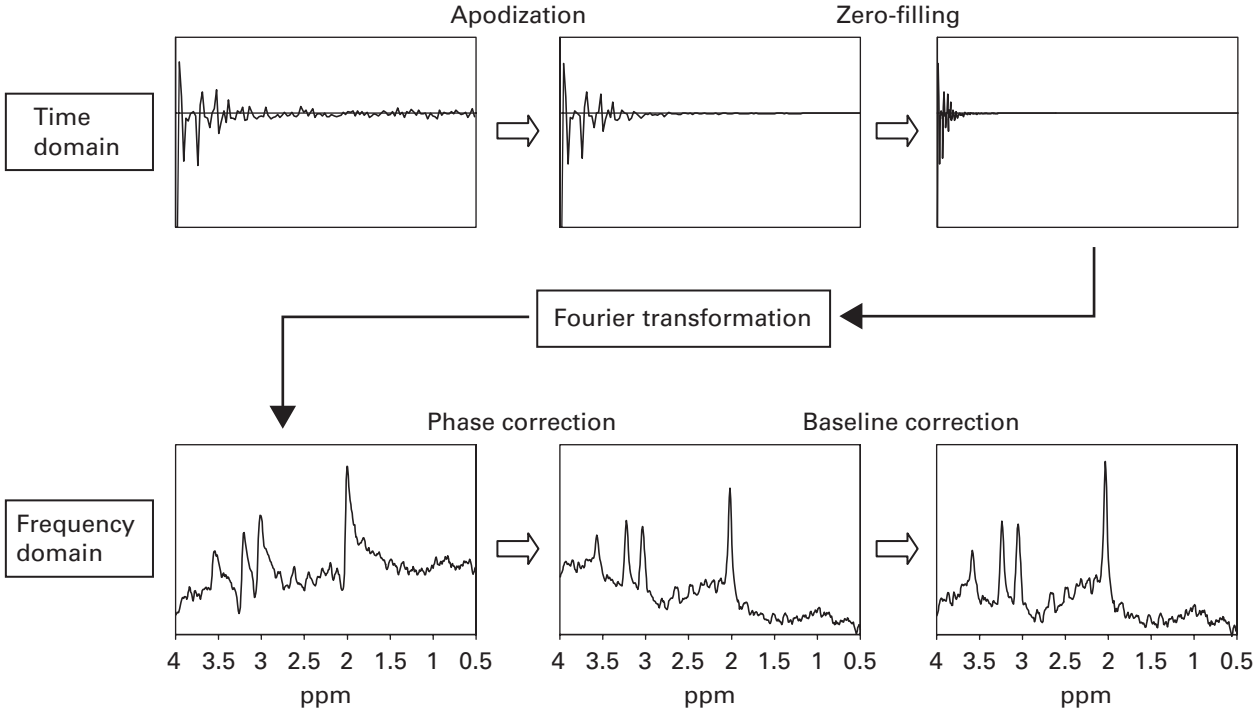

Fig. 2.2 Overview of the major processing steps for spectral analysis. The graphs show the typical appearance of MR signals (top row) and spectra (bottom row) after each step. Several pre-processing steps are performed in the time domain. Correction for gradient-induced eddy currents and removal of residual water signal yields the signal shown in the top left graph. This signal is multiplied with a decaying function ("apodization" or "low-pass filtering") and padded with zeroes on the right side of the graph ("zero-filling"; result shown in top right box). For frequency-domain processing, the pre-processed signal is Fourier transformed. The resulting spectrum typically has distorted line shapes (bottom left), which can be adjusted with a phase-correction algorithm (bottom center). Next, baseline correction (manual or automatic) yields a spectrum with a well-defined, horizontal baseline (bottom right). This pre-processed, phase- and baseline-corrected spectrum is then used to estimate metabolite peak areas with integration or iterative peak fitting algorithms.

Phase correction

The phase of the raw spectrum after Fourier transformation is usually incorrect, i.e. metabolite peaks may be inverted or have distorted line shapes (Figure 2.2, bottom left), and requires manual or automatic adjustment.

Baseline correction

After phase correction, the baseline of the resulting spectrum is typically distorted or slanted, and has to be corrected. For manual baseline correction, the user defines several spectral points, typically between the major metabolite peaks, as "baseline". The computer then fits and subtracts a smooth curve through these points. The result is a spectrum with a flat baseline, which is better suited for determination of metabolite peak areas (cf. next step).

Determination of metabolite peak areas

The final step in spectral processing is the determination of the metabolite peak areas. The signal strength S_m of each metabolite relates to the size of the metabolite signal in the time domain (e.g. in millivolts). In the frequency domain, the corresponding measure is the area of the metabolite peak. Of note, the peak height alone does not represent the metabolite concentrations.

Manual or automatic integration

One of the most intuitive and earliest methods to determine peak areas is by means of numerical integration, either manually or automatically. The user or a computer program selects two frequency points, one to the left and one to the right of a metabolite peak. The amplitude at these two points is assumed to define the spectral "baseline" and set to zero. The computer then proceeds to integrate the area under the peak, using a numerical integration algorithm.

While peak integration is very intuitive, it has substantial limitations, especially when applied to in vivo spectra. First, because in vivo spectra are commonly crowded and contain many overlapping metabolite peaks, it may be difficult to define the exact boundary between adjacent peaks. For instance, the choline (Cho) and creatine (Cr) peaks in proton spectra are separated by only 0.2 ppm, and there is often no clear boundary between the two. Of even greater concern is the overlap between some of the singlet resonances with broader multiplets or macromolecule resonances, such as that of the *N*-acetyl aspartate (NAA) peak at 2 ppm with the broad multiplet from glutamate (Glu) and glutamine (Gln) (between 2.0 and 2.4 ppm; visible at short echo times (TE)). In this situation, it is virtually impossible to separate the contributions from the different metabolites with simple peak integration algorithms.

Peak fitting

To resolve the problems of numerical peak integration, sophisticated computer algorithms have been developed that rely on the iterative fitting of ideal or experimental model spectra to in vivo spectra. Early algorithms commonly modeled in vivo spectra as a superposition of multiple individual peaks of a certain "ideal" line shape. For instance, one may assume that a given in vivo spectrum comprises multiple resonances of a Lorentzian line shape, and model it accordingly. Other common line shapes include Gaussian or variable mixtures of Lorentzian with Gaussian lines, which resemble Voigt functions.

Incorporation of prior knowledge in fitting algorithms

An important feature of the fitting algorithms is the inclusion of prior knowledge. The simplest algorithms fit each spectral peak separately. Such an approach may be sufficient for analyzing spectra that contain only a few well-separated resonances, such as long TE proton spectra of the brain. However, it is generally advantageous to incorporate "prior knowledge" into fitting algorithms. "Prior knowledge" characterizes known information about spectral characteristics that are not variable among subjects, such as relative peak positions, relative intensity or phase of peaks for multiplets, etc. The use of prior knowledge reduces the number of free parameters that need to be determined by the fitting algorithm, and generally improves the quality of the fit and reduces fitting errors.

Time-domain fitting

While less intuitive than spectral fitting in the frequency domain, the actual fitting procedure may also be performed in the time domain. In fact, mathematically there is no substantial difference between frequency- and time-domain fitting. However, in the time domain, it is essentially impossible to perform manual phase or baseline correction.

Fitting of model spectra

A more recent program named linear combination model ("LC model") (Provencher, 1993) fits in vivo spectra as a linear superposition of high-resolution "basis" spectra that are acquired from model solutions of metabolites that are present in the organ of interest. For instance, to model brain ^{1}H MR spectra, an LC model basis set may include high-resolution spectra of the major metabolites NAA, Cr and phosphocreatine, Cho, myo-inositol (mI), and Glu, as well as those of minor metabolites, such as Gln, gamma-amino-butyric acid (GABA), glucose, NAA–Glu (NAAG), etc. The fitting program determines the contribution of each basis spectrum to a given in vivo spectrum, and thus determines the relative concentration of the various metabolites in the basis set. Advantages of LC model are that all pre-processing steps, automatic phase correction as well as modeling of a smooth baseline are included. The initial acquisition of the basis spectra requires substantial expertise and effort; however, standardized basis sets are available for the most common clinical MR machines (both 1.5 and 3 T).

Common problems

Most difficulties with spectral analysis are related to the fact that in vivo spectra contain multiple overlapping peaks including those from macromolecules, have relatively low signal-to-noise ratio (SNR) and ill-defined or slanted spectral baselines. While the resonances of metabolites at high concentration, such as Cr, are generally sufficiently well defined to allow accurate peak area determination, it may be difficult or impossible to obtain reliable peak areas for minor resonances. For instance, it is essentially impossible to obtain a reliable estimate of the amount of GABA from a regular in vivo ^{1}H brain spectrum, since the major GABA signals co-resonate with the NAA and Cr resonances, which have 5–10 times higher concentration than GABA. In fact, some analysis programs determine a fitting error for each metabolite. An error of 20% or greater generally indicates that the peak area determination is unreliable; errors of 50% or greater imply that the area measure is entirely meaningless.

Quantification

Theoretical considerations

After metabolite peak areas have been determined with one of the methods described above, the second major step is to convert the peak areas, which are in arbitrary units, into metabolite concentrations. This quantification step relies on the fact that the strength of the MR signal S_m for a given metabolite "m" (or water) is proportional to the number of observed spins in the volume V of interest (VOI or voxel), which in turn is proportional to the concentration c_m of the metabolite and the number n_s of spins contributing to the resonance (e.g. 2 for water, which has 2 hydrogen nuclei). Formally, we can write for the signal of subject i at time t:

$$S_m(i,t) = \beta(i,t) \times c_m \times V \times n_s \times F_m(T_{1m}, T_{2m}, J_m, TR, TE, B_1(t)) \quad (2.1)$$

where $\beta(i,t)$ is a scaling factor and F_m is a "modulation" factor; both of these are discussed in detail below. Eq. (2.1) yields the following solution for the metabolite concentration c_m:

$$c_m = S_m(i,t)/[\beta(i,t) \times V \times n_s \times F_m(T_{1m}, T_{2m}, J_m, TR, TE, B_1(t))] \quad (2.2)$$

This equation shows that the metabolite concentration is proportional to the MR signal strength S_m and inverse to the volume, the number of spins, and the scaling and modulation factors.

The modulation function F_m describes how the signal is modulated by the TE, recovery time (TR), the longitudinal and transverse relaxation times of the metabolite (T_{1m} and T_{2m}), the radio-frequency (RF) field strength B_1 (i.e. flip angles), as well as the coupling constant J_m of the metabolite (if present). Some metabolites have simple, singlet spectra which do not contain couplings, whereas other have complicated spectral patterns with multiple coupling constants among the different protons in the molecule. The detailed dependence of F_m on these parameters may be very complicated, depends on the pulse sequence being used, and requires quantum mechanical calculations for coupled (i.e. $J_m > 0$) spin systems (Ernst *et al.*, 1990). However, the overall dependence of F_m on flip angles, relaxation times, and sequence timing (TE and TR) resembles that of MR imaging sequences in that shorter TR values or longer TE values generally attenuate metabolite signals, and act similarly to "T_1 weighting" or "T_2 weighting" in MRI. Likewise, the signal amplitude is dependent on the strength of the RF field (i.e. flip angles); maximum signal is only achieved when the RF field is adjusted correctly. Of note, since the relaxation times and J-coupling constants differ among metabolites, the factor F_m may vary from one metabolite to another.

Another important parameter in Eq. (2.1) is the scaling factor $\beta(i,t)$. The scaling factor describes how the amplitude of the observed nuclear MR (NMR) signal relates to tissue-specific "internal" variables, such as metabolite concentrations, volume, etc. β depends on the parameters such as the size of the object to be imaged, the RF coil tuning and matching, and the gain of the RF receiver chain, all of which are difficult to control. Therefore, $\beta(i,t)$ may vary from subject to subject (index i), as well as

within a subject from one study to another (i.e. over time t).

The goal of quantification is to derive the concentration c_m of a metabolite of interest from its signal strength S_m for a given subject and study. Therefore, according to Eq. (2.1), it is necessary to determine the scaling factor $\beta(i,t)$. Essentially all techniques rely on measuring the signal of a substance with known concentration (a "reference") to determine $\beta(i,t)$. Several authors have reviewed quantification techniques (Tofts and Wray, 1988; Buchli *et al.*, 1994). The subsequent paragraphs briefly describe the different choices for the "reference", and how the calibration is performed. For simplicity, we assume that a single-voxel proton MRS experiment is performed; the principles described can, however, be extended to multi-voxel methods, such as spectroscopic imaging (SI), or other nuclei.

Techniques for quantifying metabolite concentrations

"Metabolite ratios": use of a metabolite as a reference

The most common approach to spectral quantification is to express metabolite levels relative to a "reference metabolite" in the same spectrum. This approach is referred to as the use of "metabolite ratios". For ^{1}H MRS, the most common reference metabolite is total Cr, and for ^{31}P MRS, phosphocreatine is the most common reference. For example, ^{1}H MRS studies of the brain frequently report results as ratios between a metabolite peak and Cr, such as the ratio of the NAA resonance to total Cr, or the "NAA/Cr ratio". Of note, "metabolite ratios" do not reflect true concentrations, unless the concentration of the reference metabolite is known.

The use of metabolite ratios has several advantages. First, because the reference signal is acquired simultaneously with the metabolite of interest, many potential sources of systematic errors in Eq. (2.2), such as the scaling factor β, the exact volume, partial volume with cerebrospinal fluid (CSF), or the flip angles (B_1), are removed. Consequently, metabolite ratios are probably the most robust of all spectral quantitation techniques. For example, the intra-subject variability of metabolite ratios in ^{1}H MR spectra of the human brain may be below 10% within a single-site, and below 15% across sites (Webb *et al.*, 1994) using similar, automated methodology. An added advantage of "metabolite ratios" is that their measurement does not require modifications to existing MRS sequences or additional series. Therefore, "metabolite ratios" may provide reliable markers of tissue biochemistry and be useful for clinical diagnosis.

However, "metabolite ratios" are associated with a significant shortcoming: it is impossible to determine whether an abnormality in a ratio is due to a change in the numerator metabolite (e.g. NAA) or in the denominator metabolite (e.g. Cr), or both. Therefore, metabolite ratios are intrinsically ambiguous and prone to misinterpretation. Nonetheless, it is a frequent implicit assumption that the concentration of the reference metabolite is constant over time or across subjects and disease conditions. For example, reduced NAA/Cr ratio in brain tissue is commonly interpreted as decreased NAA concentration due to neuronal loss. However, reduced NAA/Cr may also be a result of increased Cr. In the brain, for instance, increased Cr concentrations (measured with one of the techniques described below) have been observed in multiple sclerosis (MS) (Inglese *et al.*, 2003), HIV dementia (Chang *et al.*, 1999), in myotonic dystrophy where the Cr concentration shows a dramatic and linear increase with the number of CTG repeats (a genetic marker of disease severity) (Chang *et al.*, 1998) and in other brain diseases. Conversely, decreased Cr concentrations are common in conditions that are associated with the destruction of normal brain tissue, such as strokes (Saunders, 2000), abscesses (Chang *et al.*, 1995), or neoplasms (Chang *et al.*, 1995; Negendank *et al.*, 1996; Preul *et al.*, 1996). Furthermore, the cerebral Cr concentration also changes during neurodevelopment (Kreis *et al.*, 1993a; Pouwels *et al.*, 1999; Horska *et al.*, 2002). Finally, Figure 2.3 demonstrates that the Cr concentration in the brain also increases during normal aging, at a rate of approximately 2.5% per decade in the white matter (WM) (Christiansen *et al.*, 1993b; Chang *et al.*, 1996; Pfefferbaum *et al.*, 1999; Suhy *et al.*, 2000).

In summary, metabolite ratios provide robust in vivo markers of biochemistry. However, metabolite ratios have to be interpreted with caution since it is

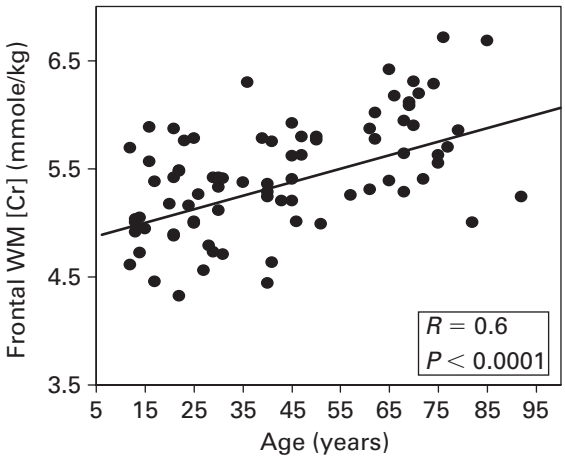

Fig. 2.3 Dependence of the total Cr concentration [Cr] in the healthy brain on age. The [Cr] in the WM increases by approximately 2.5% per decade throughout the adult life. Consequently, it is incorrect to assume that [Cr] is constant when interpreting metabolite ratios. For instance, the NAA/Cr ratio in a 65-year-old subject would be 10% lower relative to a 25-year-old subject as a result of the changes in [Cr], even without changes in the NAA concentration.

generally incorrect to assume that the concentration of the reference metabolite is unchanged across subjects and disease conditions.

Use of spectrum from control region as a reference

One clinically useful method to assess metabolite levels may be to express metabolite levels in a region of interest (ROI) relative to those in another region, for instance, a contralateral region (cf. Figure 2.1). This may be particularly useful for studies of focal abnormalities, and is commonly employed with chemical shift imaging (CSI). However, this approach provides little value in the evaluation of diseases that have a diffuse or global spatial distribution.

Use of water as a reference signal

To resolve the ambiguities associated with the use of metabolite ratios, the water signal from brain parenchyma is commonly used as a reference to determine the scaling factor β (Barker *et al.*, 1993; Christiansen *et al.*, 1993a; Ernst *et al.*, 1993). Since the water content in a unit volume of brain tissue is almost a constant, the water signal is a good internal reference for measuring metabolite concentrations. Since the water concentration in tissues are known accurately, the signal strength of the water signal can then be used to determine the scaling factor β for each subject and study, according to Eq. (2.1). The concentration of pure water is approximately 55 M, and since there are 2 protons per water molecule, the proton concentration is 110 M. In brain, the water content varies from 70% to 80% for WM and gray matter (GM), respectively, and therefore the proton concentration in brain is typically in the range of 77–88 M. Furthermore, because the water and metabolite signals are acquired from an identical VOI, and with the same pulse sequence and flip angles, many potential error sources are eliminated and the metabolite concentration measurement becomes relatively robust. An added benefit is that the time to acquire the water signal is negligible, and that it requires no substantial modifications to the MRS sequence.

One of the potential drawbacks of this approach is that the water signal is invariably acquired at an TE greater than zero, typically >20 ms. As a result, the water signal always has some degree of "T_2 weighting", and changes in the transverse relaxation time of tissue water (T_2) may lead to erroneous changes in the apparent water signal amplitude, and thus the scaling factor β. Despite this drawback, the robustness of using a single unsuppressed water FID as a reference signal has been demonstrated in a multisite study that involved identical MR machines; typical variations in metabolite concentrations were approximately 15% (Soher *et al.*, 1996).

However, the use of the water signal as a concentration reference is more complex as it may appear. Relatively large size of MRS voxels (typically cm^3) makes it likely that each voxel contains a mixture of several compartments. For instance, a typical MRS voxel in the human brain may contain GM, WM, as well as CSF; cf. basal-ganglia voxel in Figure 2.4. Each of these macroscopic compartments may contain a different concentration of each metabolite. This effect is particularly pronounced for CSF, which has markedly lower concentrations of the major brain metabolites (NAA, Cr, Cho, and mI) than brain tissue. As a result, significant amounts of CSF in a given MRS voxel may lead to an apparent reduction in metabolite concentrations, even if the